REAL TIME CONDITION MONITORING OF CHEMICAL BATTERIES

by

ANAHITA BANAEI

Presented to the Faculty of the Graduate School of

The University of Texas at Arlington in Partial Fulfillment

of the Requirements

for the Degree of

DOCTOR OF PHILOSOPHY

THE UNIVERSITY OF TEXAS AT ARLINGTON

August 2010

ACKNOWLEDGEMENTS

I would like to take this opportunity to thank several people who have contributed to my successful completion of this dissertation. First, I would like to thank my academic supervisor Dr. Babak Fahimi for his support and guidance over the past three years. It has been an honor working with him during my PhD program and a wonderful life experience.

I would like to thank Dr. Siamak Ardekani, Dr. Rasool Kenarangui, Dr. Michael Manry and Dr. Wei-Jen Lee for their agreement to be on my committee and valuable suggestions and comments.

My sincere appreciation goes to the members of the Renewable Energy and Vehicular Technology Lab at the Universty of Texas at Arlington for being supportive throughout the course of my Ph.D. work at UTA. It was my honor to be one of the members to set up and develop this lab with Dr. Fahimi and is an experience I shall always be proud of.

My gratitude goes to my family in the US and in Iran, without whose support I would have never made it this far. I am grateful to my family for the sacrifices they have made in order to provide me peace of mind, permanent support and encouragement during my long years of education.

Finally; I would like to thank my dear husband, Amir, for giving me strength and driving force towards success over the past six years. No words can express how much I appreciate the encouragement his presence has provided. I thank him for his patience, supporting me emotionally and for being ready for my challenges. To him, I dedicate this dissertation.

July 19, 2010

ABSTRACT

REAL TIME CONDITION MONITORING OF CHEMICAL BATTERIES

ANAHITA BANAEI, PhD

The University of Texas at Arlington, 2010

Supervising Professor: Babak Fahimi

Li-Ion batteries are suitable rechargeable choices for electric and hybrid electric vehicle (EV/HEV) applications due to their relatively high level of energy and power density. One of the important issues in automotive batteries is to monitor their online state-of-charge (SOC) and state-of-health (SOH).Hence, development of an efficient method for monitoring their online state-of-charge (SOC) and state-of-health (SOH) is of high importance for vehicular applications. Open circuit voltage, as one parameter used for predicting the SOC of the battery, is not readily available during charge and discharge cycles. A wide variety of research has been done on SOC and SOH estimation techniques for the automotive batteries. Most of these researches rely upon open circuit voltage of the battery.

This dissertation focuses on the state-of-charge and state-of-health monitoring of chemical batteries while the battery is under load. Also, a battery management system (BMS) to monitor the temperature, voltage and current of a battery pack has been developed. This BMS has been used to validate the proposed method of health monitoring. The method

introduced in this dissertation is based on the impulse response of the battery. Initially the impulse response of the battery is captured using a series of diagnostic experiments and the System Identification Toolbox from MATLAB®. The impulse response includes the behavioral characteristics of the battery and varies based on the specific properties of the battery such as the amount of remained charge (SOC), the amount of available charge or in other words the health status of the battery (SOH) and test conditions like temperature and current magnitude.

In order to detect the health status, various possible faults which can occur inside a battery have been identified. The behavior of the battery under different faults has been simulated and investigated using the Battery Design Studio® software. Using this software the access to the chemical characteristics of the battery is possible and internal changes corresponding to different faults can be modeled.

The impulse responses corresponding to various SOCs and also different faults are calculated and stored in a look-up table. They are used to calculate the output voltage of the battery. By comparing the calculated and the measured voltage from terminals of the battery, the SOC and SOH of the battery are estimated.

Although the focus of the research in this dissertation is on the Li-Ion batteries, the developed method can be used for other types of chemical batteries. The above mentioned steps have been supported by simulation and experimental results.

TABLE OF CONTENTS

ACKNOWLEDGEMENTS iii

ABSTRACT iv

LIST OF ILLUSTRATIONS ix

LIST OF TABLES xii

Chapter Page

1. INTRODUCTION 1

1.1 Importance of Batteries in EV/HEVs 1

1.1.1 Battery choice for EV/HEVs 2

1.2 Fundamentals of Li-Ion batteries 3

1.2.1 Li-Ion battery characteristics 5

1.2.2 State-of-charge and state-of-health definitions 6

1.2.3 Electromotive force modeling and measurement 7

1.3 State-of-the-Art 10

1.4 Objectives of the Study 12

1.4.1 Development of a method to model the Li-Ion battery 12

1.4.2 Development of the state-of-health monitoring method 12

1.4.3 Development of the state-of-charge estimation method 12

1.4.4 Development of an experimental test bed and a battery management system 13

1.5 Outline of the Dissertation 13

2. IMPULSE RESPONSE MODELING 15

2.1 Battery Modeling Methods 15

2.2 Fundamentals of the Impulse Response Modeling Method 17

2.2.1 ARMAX modeling 18
2.2.2 Calculation of the impulse response 19
2.3 Simulation and Experimental Results 22
3. STATE-OF-HEALTH ESTIMATION USING IMPULSE RESPONSE 28
3.1 Fault Classification 28
3.1.1 Electrolyte decomposition 28
3.1.2 Formation of surface films on positive electrode 29
3.1.3 Internal short circuit (soft short) 30
3.2 Fault Simulation and Analysis 33
3.3 State-of-health Estimation Method 36
3.3.1 Method description 36
3.3.2 Comparison method 38
3.3.3 Simulation results 39
3.3.4 Experimental results 43
4. STATE-OF-CHARGE ESTIMATION USING IMPULSE RESPONSE 47
4.1 Impulse Response Dependency on the State-of-charge 47
4.2 State-of-charge Estimation Method 49
4.2.1 Method description 49
4.2.2 Experimental results 50
4.3 Battery Management System Development 54
4.4 Test bed Development 57
4.4.1 The battery model 58
4.4.2 Developed battery management system for the test bed 59
4.4.3 Experimental results 64
5. CONCLUSIONS 68
REFERENCES 70

BIOGRAPHICAL INFORMATION 75

LIST OF ILLUSTRATIONS

Figure Page

1.1 Energy density map of various battery chemistries 4

1.2 The schematic of a Li-Ion cell 5

1.3 Cylindrical structure of a Li-Ion rechargeable battery 6

1.4 The schematic representation of the EMF-SOC relationship parameters. 9

2.1 The equivalent circuit of a rechargeable battery 16

2.2 Examples of equivalent circuit modeling. (a) second order equivalent circuit model and (b) forth order equivalent circuit model 17

2.3 ARMAX model structure 19

2.4 Impulse response demonstration. (a) applied pulse of current and (b) output voltage of the battery. 20

2.5 Atypical input for the system 21

2.6 Impulse response of 18650 Li-Ion battery, SOC = 80% 23

2.7 Charging pulse of 1sec for different current magnitudes: 0.5A, 1A and 1.5A, SOC = 80% 23

2.8 Comparison between measured and calculated voltages using the battery impulse response for 18650 Li-Ion battery for one discharging pulse, SOC = 100%. (a) applied current and (b) output voltages 25

2.9 Comparison between measured and calculated voltages using the battery impulse response for 26650 Li-Ion battery for two discharging pulses, SOC = 100%. (a) applied current and (b) output voltages. 26

2.10 Comparison between measured and calculated voltages using the battery impulse response for 26650 Li-Ion battery, SOC = 100%. (a) applied current and (b) output voltages. 27

3.1 Schematic representation of an aged Li-Ion battery 30

3.2 Simple equivalent circuit model for a shorted battery 32

3.3 The effect of reducing cathode active area on the voltage response to discharging current pulse of1A for 1s, SOC = 70% 34

3.4 The effect of electrolyte density reduction on the voltage response to discharging

current pulse of1A for 1s, SOC = 70% 34

3.5 The effect of change in current magnitude on the voltage response for two different fault situations 35

3.6 State-of-health estimation algorithm 37

3.7 The pattern recognition block in detail 38

3.8 Method validation for the battery with the fault of reduced active area of the positive electrode by 40% for two discharging current pulses. (a) applied current waveform and (b) comparison of measured and calculated voltages 41

3.9 Method validation for the battery with the fault of reduced active area of the positive electrode by 40% for one discharging current pulse 41

3.10 Method validation for the battery with the fault of electrolyte density reduction by 70%. (a) first comparison and (b) second comparison 43

3.11 Comparison of the measured output voltage of the healthy battery and the calculated voltages of the faulty and healthy batteries, SOC = 100%. (a) voltage comparison for pulse length of 10s and (b) voltage comparison for two pulses 45

3.12 Comparison of the measured output voltage of the faulty battery and the calculated voltages of the faulty and healthy batteries, SOC = 100%. (a) voltage comparison for pulse length of 10s and (b) voltage comparison for two pulses 46

4.1 Comparison of the impulse responses for various SOCs 30%, 50%, 70% and 90%, for applying a charging current pulse of 1A 48

4.2 Impulse responses of the experimental cell for various SOCs 49

4.3 Block diagram of the state-of-charge estimation method 50

4.4 Applied current and measured voltage of the experimental cell, SOC = 20% 51

4.5 Calculated impulse response of the experimental battery, SOC = 60% 51

4.6 Comparison of the measured voltage of the battery for SOC = 100% with the calculated voltages for SOCs of 100%, 60% and 20% 52

4.7 Comparison of the measured voltage of the experimental battery for SOC = 60% with the calculated voltages for SOCs of 100%, 60% and 20% 53

4.8 Comparison of the measured voltage of the experimental battery for SOC = 20% with the calculated voltages for SOCs of 100%, 60% and 20% 54

4.9 Comparison of the measured voltage of the experimental battery for SOC = 20% for two discharging cycles with the calculated voltages for SOCs of 100%, 60% and 20% 54

4.10 Block diagram of the monitoring circuit 55

4.11 The battery monitoring system for a battery pack containing six18650 Li-Ion cells. (a) designed Battery Management System board, (b) TMS320F2812 DSP board and (c) overall connections of the power supply, battery pack and controller. 57

4.12 The SE180AHA Li-Ion battery specifications. (a) battery specifications and (b) the experimental battery. 59

4.13 The cell configuration for 40kwh battery pack 59

4.14 The schematic of the developed battery management system 60

4.15 The battery management system boards 61

4.16 The overall view of the experimental test bed. 62

4.17 the experimental test bed. (a) battery pack, BMS boards, touch screen and power supply and (b) the load and current sensor 63

4.18 Comparison of the measured and calculated voltages for the cell with SOC of 90% for two discharging pulses. (a) applied current waveform and (b) voltage comparison. 65

4.19 Comparison of the measured and calculated voltages for the cell with SOC of 90% for one discharging pulse. (a) applied current waveform and (b) voltage comparison. 66

4.20 Comparison of the measured and calculated voltages for the cell with SOC of 50%. (a) voltage comparison for two discharging current pulses and (b) voltage comparison for one discharging current pulse. 67

LIST OF TABLES

Table Page

1.1 Comparison of the characteristics of different battery chemistries 3

CHAPTER 1

INTRODUCTION

In this chapter a description of the motivations, methods, and objectives of this dissertation is presented. First, the importance of Li-Ion batteries in vehicular and renewable energy systems has been discussed. Then the issues regarding the health monitoring and fault detection in this family of electrochemical batteries are explored. The state-of-the-art along with their advantages and disadvantages are surveyed. This chapter is concluded by an overview of the dissertation outline and objectives.

1.1 Importance of Batteries in EV/HEVs

Interest in Electric and Hybrid Electric Vehicles (EV/HEV) and plug-in Vehicles (PHEV) has grown in recent years in response to rising fuel costs and increased concern about pollution and global warming. New environmental concerns about the amount of pollutants entering the atmosphere by the Internal Combustion Engine (ICE) of the automobiles create an effective motivation to this emerging technology. Also, the efficiency of the internal combustion engine is about 20% in an average driving scenario, while for an electric vehicle the overall electric drive efficiency can reach a peak value of about 80%. So, the problems associated with conventional ICE automobiles are environmental as well as economical. All these Concerns force governments all over the world to consider alternative vehicular technologies.

Electric Vehicle (EV) uses one or more electric motors for propulsion and the energy used to power the motor is obtained from an energy storage system which mostly is a battery. A Hybrid Electric Vehicle (HEV) combines the Internal Combustion Engine (ICE) with an electric motor to form the propulsion system. Thus, besides the need for fossil fuels as the energy resource for ICE, another energy storage system is required to provide energy for the electric motor. Energy storage system is an important component in EV/HEVs and batteries are the

primary option for the energy storage system. Hence, the demand for rechargeable batteries has witnessed an increase as well. The battery system choice is very crucial for EV/HEVs and it requires satisfying important characteristics like high performance and high reliability. Commercially available batteries do not fully meet these performance requirements. Thus there is a need to develop new battery management system with improved performance and advanced monitoring technologies with characteristics such as high energy and power densities, long life, low cost, little maintenance and a high degree of safety. While accelerating a hybrid vehicle a large amount of energy is required to be taken out of battery during a short period of time. So the battery needs not only to store a large amount of energy but also to be able to deliver considerable energy in a short time (high power) [1].

1.1.1. Battery choice for EV/HEVs

Battery performance requirements for EV/HEV applications are:

- High specific energy and energy density to provide adequate vehicle driving range.
- High power density to provide acceleration.
- Long cycle life with manageable maintenance.
- Low cost.

Initially, lead-acid batteries were used as the energy storage system in EV/HEVs, but new improvements in battery technologies have made Ni-MH and Li-ion batteries the common choice for the mentioned application. Table 1.1 shows a comparison of various types of batteries from different points of view. Rechargeable batteries are severely competing one another for high energy density and high rate characteristics on demand from the market. Ni-MH battery was released in the market in the late 1990 as a high capacity with the voltage compatibility with Ni-Cd battery. Although Ni-MH is relatively compact compared with Ni-Cd battery, Li-Ion battery has more advantage in that point as shown in Table 1.1. Li-Ion and Ni-MH batteries are predominant batteries in terms of energy density, power density and economics, but not safety. Li-Ion batteries continue to proceed for high capacity and cost effectiveness.

Figure 1.1 shows the comparison of the batteries in case of energy density. Their energy density area began to overlap with that of the other batteries in a consequence as shown in Figure 1.1 [2].

Table 1.1 Comparison of the characteristics of different battery chemistries.

	Lead-Acid	**Ni-Cd**	**Ni-MH**	**Li-Ion**
Specific energy density (Wh/Kg)	30-50	45-80	60-120	110-180
Energy density (Wh/L)	10-100	30-150	100-300	200-600
Power density (W/Kg)	400	600	600	1800
Dimension (mm)	16.5 x 66.5	16.5 x 66.5	16.5 x 66.5	18 x 65
Capacity (Ah)	1.5	1.5	3.5	1.4
Voltage (V)	2.1	1.2	1.2	3.7
Self-discharge (%/month at 20^{o}C)	?	25	< 20	12
Max. current (A)	20C	3C	0.6C	2C
Cycle life (cycle)	> 300	> 500	> 500	> 500
Memory effect	No	Yes	Yes	No
Energy cost [Wh/$]	5 - 8	2 – 4	1.4 – 2.8	3 - 5

1.2 Fundamentals of Li-Ion Batteries

Li-Ion batteries have high power density comparing to other chemistries and this property along with other advantages of this batteries make them the main contenders for energy storage system in EV/HEVs. Some of the capabilities of Li-Ion batteries are as follows:

- high voltage
- high energy density
- high power density

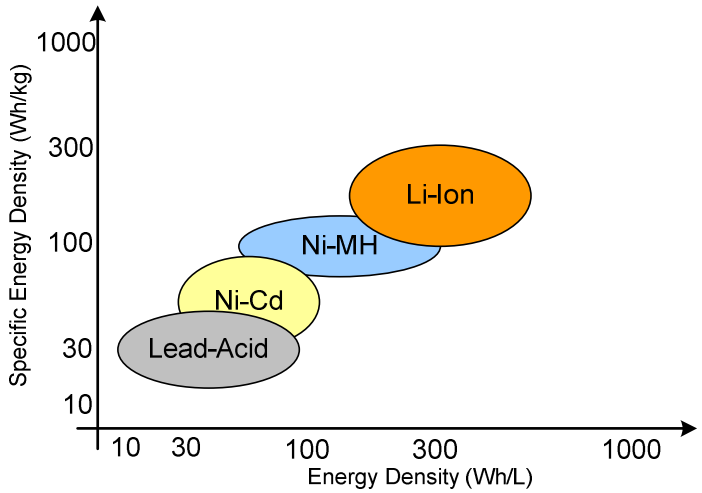

Figure 1.1 Energy density map of various battery chemistries.

- low self-discharge
- fast charging
- high energy-to-weight ratio
- wide operating temperature
- durability if charged properly
- no memory effect

One of the characteristics of Li-ion batteries which make them outstanding among other types of batteries is that they hold their charge better. A Li-ion battery loses a small percentage of its charge comparing to other types of batteries. They are generally lighter than other types of batteries of the same size and they don't have memory effect. Memory effect happens when battery charges and discharges repetitively with shallow depth of discharge. Li-Ion batteries can be used continuously for various depth of discharge without causing any problem, which means there is no need to discharge them completely before recharging. All these capabilities of Li-ion batteries are the main reason to make these type of batteries the future choice of energy storage systems for EV/HEVs. There are certain disadvantages for this type of battery like moderate discharge current and high cost [3]. They are also sensitive to high temperature and

ignite or explode when exposed to high temperature. They are in danger of ignition or explosion if short-circuit or any attempt to open the case occurs. For this reason, they are normally included safety devices and their temperature should be monitored carefully. Hence, the focus of this dissertation is on SOH and SOC monitoring in Li-Ion batteries.

1.2.1 Li-Ion battery characteristics

Li-Ion batteries are a type of rechargeable battery in which a lithium ion moves between anode and cathode during charge and discharge. Figure 1.2 shows a schematic of a typical Li-Ion battery. A cell consists of five regions: the negative electrode current collector made of copper, the porous composite positive electrode, the porous separator, the porous composite positive electrode and the positive electrode current collector made of aluminum. The composite electrodes are made of their active material particles, held together with a PolyVinyliDene Fluoride (PVdF) binder and a suitable filler material such as carbon black to enhance the electronic conductivity.

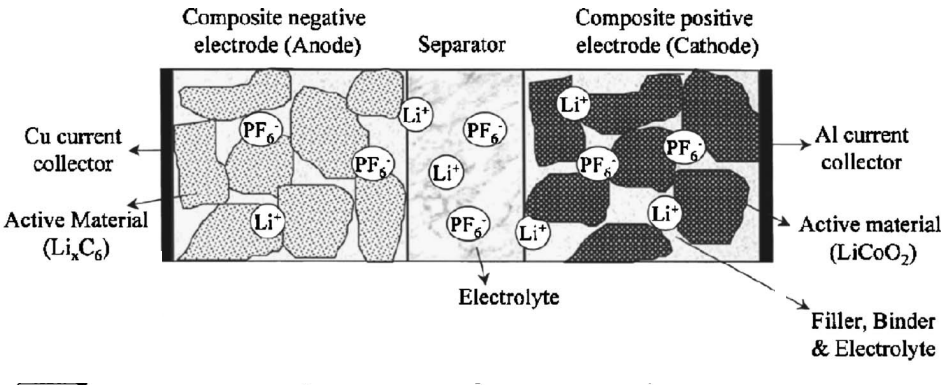

Figure 1.2 The schematic of a Li-Ion cell (courtesy of [4]).

The positive electrode is generally composed of a lithium metal oxide such as $LiCoO_2$, $LiNiO_2$ and $LiMn_2O_2$. The negative electrode is a carbon-based material which is normally made of graphite. The electrolyte consists of lithium salts dissolved in a solvent such as $LiPF_6$, $LiBF_6$ or $LiClO_4$ to act as a carrier, conducting lithium ions between anode and cathode [4, 5]. The

typical reaction taking place in cathode is as follows:

$$LiCoO_2 \Leftrightarrow Li_{1-x}CoO_2 + xLi^+ + xe^- \quad (1.1)$$

The reaction in anode can be shown as below:

$$xLi^+ + xe^- + 6C \Leftrightarrow Li_xC_6 \quad (1.2)$$

During discharge the lithium ions separates from the negative electrode active materials and enter the solution phase, while in the positive electrode lithium ions from the solution phase intercalate into the $LiCoO_2$. Figure 1.3 illustrates the cylindrical cell structure of the Li-Ion battery.

The operating voltage range is critical for Li-Ion batteries since they are sensitive to deep discharge or overcharge and extremely high or too low SOC can lead to irreversible damage in the battery. So, monitoring the voltage of the battery is an essential task for battery management systems.

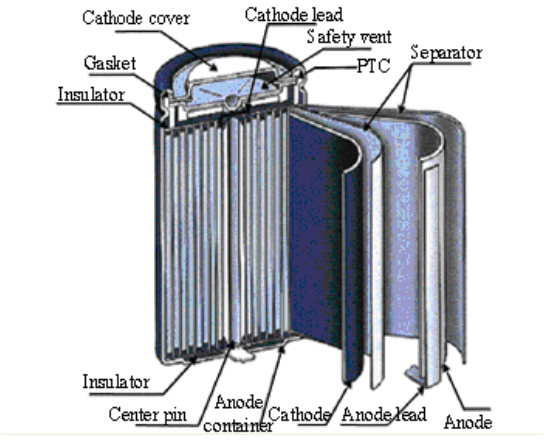

Figure 1.3 Cylindrical structure of a Li-Ion rechargeable battery (courtesy of Battery Design Studio®).

1.2.2 State-of-charge and state-of-health definitions

One of the important issues in automotive batteries is to monitor their online State-of-Charge (SOC) and State-of-Health (SOH) due to problems caused by poor battery maintenance. State-of-Charge of the battery is an indicative of the amount of charge remained

inside the battery. An accurate and reliable SOC estimation method is very important in effective management of the energy within the vehicle. An accutare assessment of SOC is very important in tehcharging process as well. This is primarily because an inaccurate SOC estimator when the battery is fully charged may lead to overcharging the battery and reducing its life time. In other case, if the battery is not charged completely and consequently it needs to be charged more frequently which again results in lower life time.

State-of-health is the ability of the battery to store and retain energy which is subject to decline by battery aging and usage pattern. During lifetime of the battery, its performance or health deteriorates gradually due to irreversible physical and chemical changes which are caused by battery usage. Deep discharging, overcharging and using the battery in high temperature are other examples of misusage of the batteries which effect on the health of the battery [6]. Some of the physical and chemical changes caused inside the battery are: accumulation of a film of electrolyte decomposition products on the surface of the cathode which results in particle isolation and increasing the internal impedance of the battery in result, chemical reactions in cathode (cathode decomposition) which isolates active materials in positive electrode and formation of passive surface films on both electrodes. As a result of all these changes the amount of available active materials or in other hand the capacity of the battery is reduced. Therefore, the battery can not deliver its maximum capacity even if it is fully charged.

Achieving an efficient and reliable battery management system is an important key in EV/HEV development. Battery management systems monitor key operational parameters, such as current, voltage, temperature, SOC and SOH. Li-Ion batteries are much less tolerant of abuse than other battery chemistries, so they particularly require precise monitoring of the charge and health status to ensure that no overcharging or deep discharging is occurred and also it is capable to deliver the specific amount of charge. Hence, one of the important issues to be considered is the prediction of state-of-charge and state-of-health.

1.2.3 Electromotive force modeling and measurement

The EMF is the internal driving force of a battery for providing energy to a load. The battery voltage only equals the EMF when no current flows and the voltage has relaxed to its equilibrium value. i.e., the EMF. In other words, the open-circuit voltage of the battery equals to the EMF.

In principle, the EMF can be calculated from thermodynamic data and the Nernst equation. The EMF-SOC relationship is important to relate the SOC of the battery to its open-circuit voltage. With this model for a certain EMF and temperature the corresponding SOC can be calculated. The EMF of a Li-Ion battery is modeled as the difference in equilibrium potentials of the positive and negative electrodes, i.e.

$$V_{EMF} = E_{eq}^{+} - E_{eq}^{-} \tag{1.3}$$

where the equilibrium potential of the positive electrode (E_{eq}^{+}) is given by

$$E_{eq}^{+} = E_0^{+} - \frac{RT}{F}[\log(\frac{x_{Li}}{1-x_{Li}}) + U_j^{+} x_{Li} - \zeta_j^{+}] \tag{1.4}$$

$$\zeta_2^{+} = (U_2^{+} - U_1^{+})x_{ph} + \zeta_1^{+}, j = \begin{cases} 1, & x_{ph} \le x_{Li} \le 1 \\ 2, & \frac{1}{2} \le x_{Li} \le x_{ph} \end{cases} \tag{1.5}$$

in which E_0^{+} is the standard potential of the $LiCoO_2$ electrode in [V], U_j^{+} is the dimensionless interaction energy coefficient in the $LiCoO_2$ electrode, ζ_j^{+} is a dimensionless constant in the $LiCoO_2$ electrode, x_{Li} the mole fraction of Li^{+} ions inside the positive electrode or in other words the SOC of the $LiCoO_2$ electrode, R the gas constant [8.314 J (mol K)$^{-1}$], F the Faraday constant (96,485 C mol^{-1}), and T the ambient temperature in [K]. In Eq. 5 a phase transition (ph) occurs at $x_{Li} = x_{ph}$ that results in a curvature change. According to modern literature on Li-Ion batteries with a $LiCoO_2$ electrode, the main phase-transition point is located near $x_{ph} \approx 0.75$ [5, 7].

The equilibrium potential of the negative electrode is modeled similarly as follows

$$E_{eq}^{-} = E_0^{-} - \frac{RT}{F}[\log(\frac{z_{Li}}{1-z_{Li}}) + U_j^{-} z_{Li} - \zeta_j^{-}] \tag{1.6}$$

$$\zeta_2^- = (U_2^- - U_1^-)z_{ph} + \zeta_1^-, j = \begin{cases} 1, & 0 \le z_{Li} \le z_{ph} \\ 2, & z_{ph} \le z_{Li} \le 1 \end{cases} \quad (1.7)$$

where E_0^- is the standard potential of the LiC_6 electrode in [V], U_j^- is the dimensionless interaction energy coefficient in the LiC_6 electrode, ζ_j^- is a dimensionless constant in the LiC_6 electrode, and z_{Li} the mole fraction of Li^+ ions inside the negative electrode or in other words the SOC of the negative electrode. In the negative electrode a phase transition occurs around $z_{ph} \approx 0.25$.

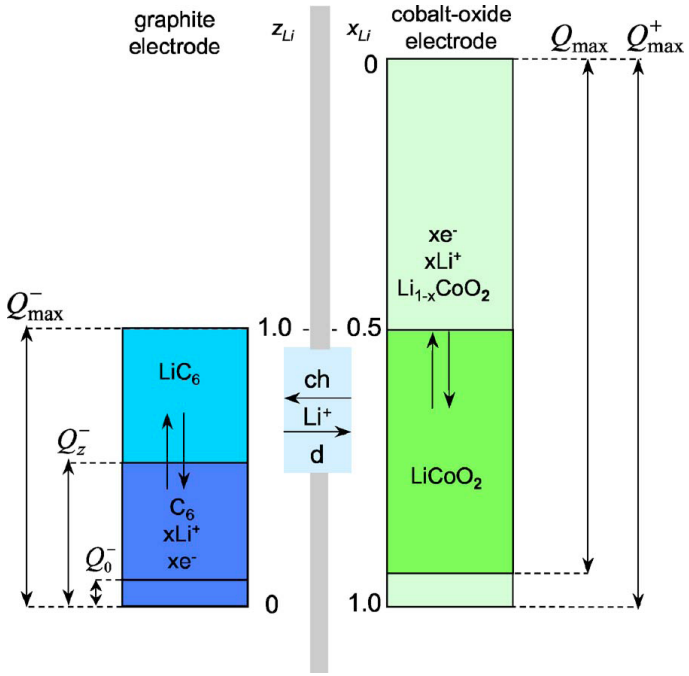

Figure 1.4 The schematic representation of the EMF-SOC relationship parameters (courtesy of [6]).

As schematically indicated in Figure 1.4, the Li-Ion battery can be characterized by the following parameters: Q_{max}^+ is the maximum capacity of the positive electrode, Q_{max}^- the maximum capacity of the negative electrode, Q_{max} the amount of electrochemically active Li^+ ions inside the battery, Q_0^- the amount of Li^+ ions inside the negative electrode in a fully discharged battery, and Q_z^- the charge stored in the negative electrode for a given SOC. Given

these parameters and SOC, the x_{Li} and z_{Li} can be determined from

$$z_{Li} = \frac{Q_z^-}{Q_{max}^-} \tag{1.8}$$

$$Q_z^- = Q_0^- + \frac{SOC}{100}(Q_{max} - Q_0^- - \frac{Q_{max}^+}{2}) \tag{1.9}$$

$$x_{Li} = \frac{Q_{max} - Q_z^-}{Q_{max}^+} = \frac{Q_{max} - z_{Li}Q_{max}^-}{Q_{max}^+} \tag{1.10}$$

The Li^+ ions move from cobalt-oxide electrode to the graphite electrode during charging. At the end of charging the battery, SOC is defined to be 100%. During discharge the Li^+ ions move from the graphite electrode to the cobalt-oxide electrode and the SOC will be 0%. Using all the mentioned equations, EMF-SOC relationship is obtained [4].

1.3 State-of-the-Art

The ongoing challenges in the design and implement of State-of-Charge and State-of-Health estimation methods have been the focus of many researches [8-26]. However improvements in these areas have been incremental. Achieving a reliable and accurate SOC and SOH estimation method is in high importance for EV/HEV applications.

A wide variety of researches have been done on the State-of-Charge estimation for electrochemical batteries. Most of them rely upon open-circuit voltage of the battery [8, 9, and 27]. Most of these methods do not take into account parameter variations in electrochemical batteries and as such their accuracy is subject to the health status of the battery, aging effects, and possible manufacturing imperfections. In addition, the open circuit voltage is not readily available while the batteries are in use. These methods are not accurate enough and as a result would jeopardize the chance of correct charging and the performance of the battery. This can potentially lead to thermal runway in Li-Ion batteries.

Another SOC estimation method is based on current integration during charge and discharge states of the battery (coulomb counting) [10]. However, the estimation error existed in each state integrates with the current and increases gradually. Measurement of the battery

internal impedance or resistance is another method which again does not provide acceptable results [11-12]. Another approach for estimating SOC of a battery is to model the electrochemical dynamics of the battery and various processes taking place inside the cell, and then using the model to predict the terminal voltage [5, 14]. However measuring all the electrical and chemical parameters of a cell would be difficult.

Several studies have been done on SOH estimation and the parameters effecting health status of Li-Ion batteries over the past few years [17-20]. A common battery monitoring method is full or partial discharge test. However this method is expensive and takes a very long time. It also damages the battery, since routine and deep (in case of full discharge) battery discharge can reduce the life of the battery. Also in partial discharge test the accuracy of the technique depends on the depth of discharge [7, 21].

Another method which is used for SOH estimation of Lead-Acid batteries uses a phenomenon referred to as *coup de fouet,* which means producing a large voltage drop in the early minutes of battery discharge. By aging the battery encounters a loss of active material utilization. This is caused by various processes such as sulfation and change in pore structure which causes decrease in active surface area and increase in local resistances. As a result of these changes the amount of available capacity decreases and the *coup de fouet* voltage is lowered [21]. Although this is a quick and simple technique for estimating SOH of the battery, it cannot be done online and it needs a constant load for performing the discharge test.

Ohmic techniques including impedance, resistance and conductance measurements are another way of SOH estimation, but these techniques are not precise [22-26]. Measuring the internal resistance of the battery is very sensitive to measurement error. The accuracy of the measurement highly depends on the way the contact is made between the battery terminals and the lead of the ohmic meter. Besides, none of the methods are efficient for real time estimation of SOH while the battery is under load. These methods require making measurements which are not always available in a general application.

1.4 Objectives of the Study

In this section the various tasks and objectives including the modeling of the Li-Ion battery, fault classification and detection, pattern recognition and experimentation are presented.

1.4.1 Development of a method to model the Li-Ion battery

There are several methods to model a Li-Ion battery such as equivalent circuit, mathematical and electrochemical modeling. A new battery modeling method based on the battery impulse response is introduced. The proposed model is represented by autoregressive moving average with exogenous input model (ARMAX) polynomial structure. Given the impulse response coefficients, the model can be a precise replacement of the battery in order to study the behavioral characteristics of the cell. Of course, the impulse response model is highly dependent to the specific parameters of the battery such as state-of-charge and state-of-health. This behavior will be used as a method to estimate the SOC and SOH of the battery.

1.4.2 Development of the state-of-health monitoring method

The ability of the battery to deliver the specified amount of charge compared to a fresh battery, known as state-of-health (SOH) needs to be monitored frequently to depict the battery performance. SOH is an indication of the battery lifetime which determines when the battery needs to be replaced. A new method of SOH estimation is developed here based on the impulse responses of the battery. A set of impulse responses of an unhealthy battery related to different faults is stored in a look up table. Comparing the output voltage of the battery with the calculated voltages using the stored impulse responses is used as a tool to predict the health condition of the battery and also the type of fault occurred inside the battery.

1.4.3 Development of the state-of-charge estimation method

Prediction of state-of-charge (SOC) is important for all battery applications. The amount of charge remained in the battery should be determined continuously in order to prevent deep discharging and realize how longer the battery can continue to perform before it needs to be

charged again. A set of impulse responses corresponding to different levels of charge can be stored in a look up table and by monitoring the output voltage of the battery the SOC can be estimated in real time.

1.4.4 Development of an experimental test bed and a battery management system

Monitoring the status of the battery is in high importance in order to prevent working in a non safe domain. It can be determined if the battery is working properly or there is any problem by sensing the temperature of the battery. Voltage and current measurements are necessary during charging process to follow the charging profile and also prevent overcharging. Voltage measurement is also required for balancing process. An electric circuit is designed and developed to monitor the specified parameters.

For the validation of the proposed scheme, an experimental battery management system was designed and developed in the Renewable Energy and Vehicular Technology Lab. This experimental system can monitor the voltage, current and temperature of six individual cells in series. The designed system is used to validate the proposed techniques. Monitoring the specific parameters, estimating the charge status and determining the health condition of the batteries are the main objectives in this experimental setup.

1.5 Outline of the dissertation

The state-of-the-art investigation, problem identification, modeling and detection of Li-Ion batteries are presented here. This dissertation includes 5 chapters whose outline is as follows:

Chapter 2 describes the fundamentals of the impulse response modeling. In this chapter the impulse response model is developed and implemented for Li-Ion batteries. To validate this model, the convolution result of the current waveform with the impulse response is compared to the measured data.

Chapter 3 deals with the fault classification of Li-Ion batteries and the conditions which lead to the mentioned faults. A novel method for state-of-health estimation based on the

impulse response will be introduced in details. The proposed method is supported by experimental and simulation results.

Chapter 4 introduces the new method for estimating the state-of-charge of Li-Ion batteries based on the battery impulse response. Experimental and simulation results are used to validate the novel method.

Chapter 5 summarizes the achievements of this study and provides concluding comments on the findings.

CHAPTER 2

IMPULSE RESPONSE MODELING

The present chapter describes various methods of modeling electrochemical batteries. A novel modeling method based on the impulse response of the battery is introduced here. This method later will be used to estimate the state-of-charge and state-of-health of Li-Ion batteries. The proposed method is supported by simulation and experimental results.

2.1 Battery Modeling Methods

Accurate battery models are needed for control strategy development and behavior investigation. Having the precise battery model, the effect of various conditions can be observed without causing any problem to the battery. Various methods have been developed for modeling a battery. Some of them are based on the electrochemical characteristics and the dynamics of the battery. A dynamic model which is able to capture the electrochemical reaction dynamics of the battery is basically in high order and too complex for a practical use of an electrical engineer. Although such type of model can be used as a baseline in order to obtain more manageable reduced order models [5, 7, 14, 28-30].

While physics-based models have been built to study the internal dynamics of Li-Ion batteries, these models are not suitable for system level design studies. For this reason, another method based on electrical properties of the battery has been emerged which is called equivalent circuit model. It provides a model to explain the voltage waveforms and to quantify the results into four circuit parameters which represent various parts of the battery. Various equivalent circuit models have been developed [27, 31-32, 33-38]. Figure 2.1 shows a typical equivalent circuit of a rechargeable battery.

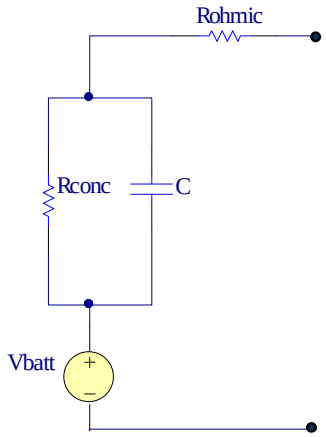

Figure 2.1 The equivalent circuit of a rechargeable battery.

R_{ohmic} represents the electrode and packaging resistance of the battery, R_{conc} represents the battery's internal resistance, which defines the maximum current a battery can deliver and accounts for charging and discharging losses. C is the capacity of the battery which is formed by series connection of the double layer capacitance formed by each pair of battery cells and is indicative of the finite amount of electric charge stored inside the battery. V_{batt} represents the battery's rated voltage at no-load (open circuit) condition. To obtain various parameters of the equivalent circuit model, various charging and discharging tests need to be made. Figure 2.2 depicts a second order and a forth order battery equivalent models [33].

2.2 Fundamentals of the Impulse Response Modeling Method

Convolution is a formal mathematical operation just like multiplication and addition. The difference is that Convolution takes two signals instead of two numbers and produces a signal. The convolution of two functions such as f and g is denoted by $f * g$ and the basic definition is given by the integral of one function at t multiplied by another function at $t - \tau$ (over the entire domain of the independent variable, i.e. time). This operation is shown below:

$$(f * g)(t) = \int_{-\infty}^{+\infty} f(\tau).g(t-\tau)d\tau = \int_{-\infty}^{+\infty} f(t-\tau).g(\tau)d\tau \qquad (2.1)$$

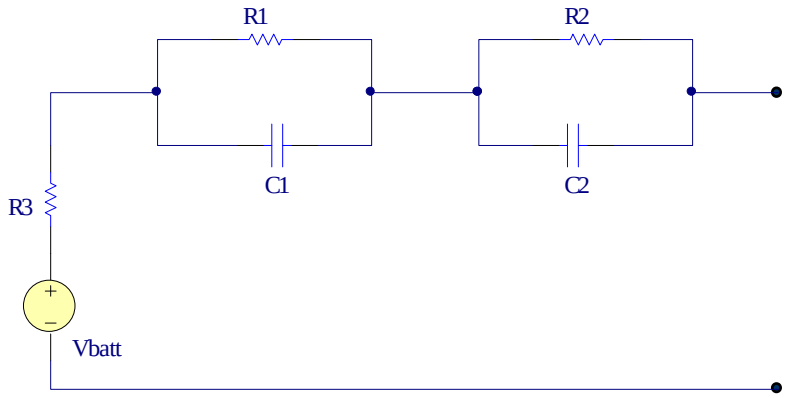

(a)

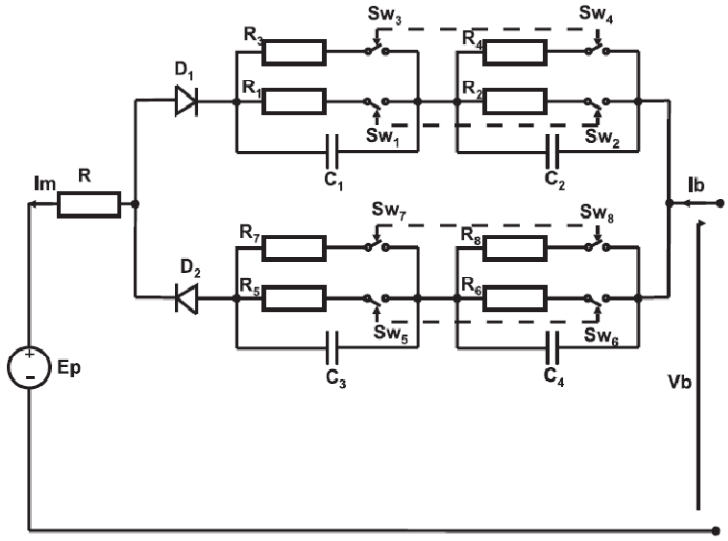

(b)

Figure 2.2 Examples of equivalent circuit modeling. (a) second order equivalent circuit model and (b) forth order equivalent circuit model (courtesy of [34]).

The convolution in discrete domain is represented as follows:

$$(\hat{f} * \hat{g})[n] = \sum_{k=-\infty}^{+\infty} \hat{f}[k].\hat{g}[n-k] = \sum_{k=-\infty}^{+\infty} \hat{f}[n-k].\hat{g}[k] \qquad (2.2)$$

Convolution has some specific mathematical properties such as commutative, associative and distributive. Commutative property states that it does not matter which function

is taken first and the order in which signals are convolved can be exchanged:

$$a[n] * b[n] = b[n] * a[n] \tag{2.3}$$

associative property of convolution describes how three signals can be convolved:

$$(a[n] * b[n]) * c[n] = a[n] * (b[n] * c[n]) \tag{2.4}$$

and distributive property indicates the parallel systems with added outputs can be replaced with a single system:

$$a[n] * b[n] + a[n] * c[n] = a[n] * (b[n] + c[n]) \tag{2.5}$$

From the linear system theory the output of a linear time invariant (LTI) system for an arbitrary input can be determined using its impulse response as shown below:

$$y[k] = x[k] * h[k] \tag{2.6}$$

where $x[k]$, $h[k]$ and $y[k]$ depict the input, impulse response and output of the system. In other words, the convolution of the input to the system with its impulse response gives the output of the system. A linear system's characteristics are completely specified by its impulse response, which is implemented by the mathematics of convolution. If two systems are different in any way, they will have different impulse responses

2.2.1 ARMAX modeling

For a single-input/single-output system (SISO), the Autoregressive moving average model (ARMAX) polynomial model structure is given by:

$$A(q)y(t) = B(q)u(t) + C(q)e(t) \tag{2.7}$$

where $y(t)$ represents the output at time t, $u(t)$ represents the input at time t, $e(t)$ is the white-noise disturbance and q^{-1} is the back-shift operator. Figure 2.3 shows the structure of the ARMAX model. The coefficients are defined as:

$$A(q) = 1 + a_1 q^{-1} + ... + a_n q^{-n} \tag{2.8}$$

$$B(q) = b_1 + b_2 q^{-1} + ... + b_m q^{-m} \tag{2.9}$$

$$C(q) = 1 + c_1 q^{-1} + ... + a_r q^{-r} \tag{2.10}$$

where n, m and r are the orders of the polynomials, respectively. The appropriate model orders should be determined in order to estimate the ARMAX model. Having the specified model, the input current of the battery can be used as the input of the model ($u(t)$) and by using the polynomials, the output voltage can be calculated ($y(t)$). Autoregressive moving average models (ARMAX) can be used to express the impulse response of a discrete time LTI system numerically [15, 39].

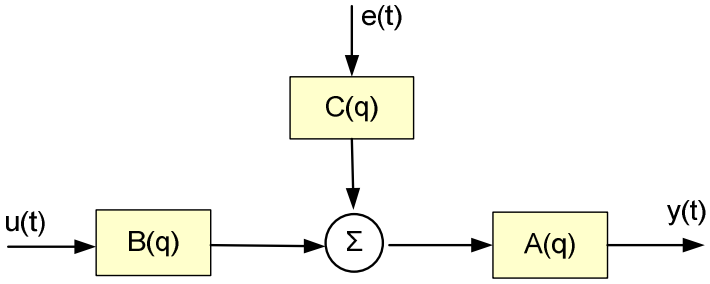

Figure 2.3 ARMAX model structure.

2.2.2 Calculation of the impulse response

The impulse response of a battery can be used as a battery model and be substituted with the battery to calculate the output voltage. In order to determine the impulse response of a battery a narrow pulse of current (with a unitary area) is applied to the battery and the output voltage is monitored as shown in Figure 2.4.

Having the impulse response of the battery and convolving it with any arbitrary input current, the output voltage can be calculated. It can be shown as follows:

$$v[k] = i[k] * h[k] \tag{2.11}$$

where $i[k]$, $h[k]$ and $v[k]$ are the battery terminal current, impulse response of the battery and the terminal voltage respectively.

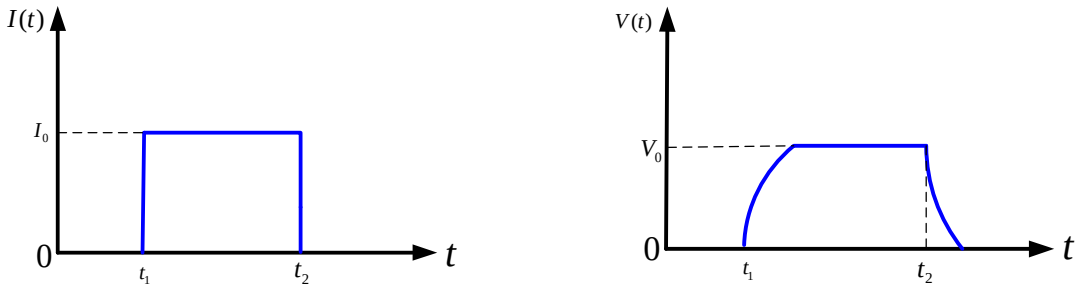

(a) (b)

Figure 2.4 Impulse response demonstration. (a) applied pulse of current and (b) output voltage of the battery.

In order to define an impulse for a specific system, suppose a first order LTI system characterized as follows:

$$\frac{dy}{dt}+\frac{1}{\tau}y=x(t) \tag{2.12}$$

where y is the output, x is the input and τ is the time constant of the system [40]. Taking the laplace transform, the transfer function of the system would be presented as:

$$H(s)=\frac{\tau}{1+\tau.s} \tag{2.13}$$

Suppose that the input of the system ($f(t)$) is defined as Figure 2.5 which is characterized as:

$$f(t)=\frac{1}{\Delta}(u(t)-u(t-\Delta)) \tag{2.14}$$

The laplace transform of $f(t)$ is calculated as follows:

$$F(s)=\frac{1}{\Delta.s}(1-e^{-\Delta s}) \tag{2.15}$$

$$=\frac{1}{\Delta.s}[1-(1+(-\Delta.s)+\frac{(-\Delta.s)^2}{2!}+\frac{(-\Delta.s)^3}{3!}+.....)]. \tag{2.16}$$

$$=1-\frac{\Delta.s}{2!}+\frac{(\Delta.s)^2}{3!}-\frac{(\Delta.s)^3}{4!}+..... \tag{2.17}$$

In order to find the response of the system to the input $f(t)$, $F(s)$ is multiplied by the transfer function of the system, $H(s)$:

$$Y(s) = F(s).H(s) = \frac{\tau}{1+\tau.s} \times [1 - \frac{\Delta.s}{2!} + \frac{(\Delta.s)^2}{3!} - \frac{(\Delta.s)^3}{4!} + ...] \quad (2.18)$$

$$= [\frac{\tau}{1+\tau.s} - \frac{\tau}{2!} \times (\frac{\Delta.s}{1+\tau.s}) + \frac{\tau(\Delta.s)}{3!} \times (\frac{\Delta.s}{1+\tau.s}) - \frac{\tau(\Delta.s)^2}{4!} \times (\frac{\Delta.s}{1+\tau.s}) + ...] \quad (2.19)$$

In order to consider $f(t)$ as an impulse, the response of the system to $f(t)$ should be equal to the impulse response of the system:

$$Y(s) = F(s).H(s) = H(s) = \frac{\tau}{1+\tau.s} \quad (2.20)$$

This means that all the terms except the first one in equation 2.19 need to be zero:

$$\frac{\Delta.s}{1+\tau.s} \to 0 \qquad \Rightarrow \qquad \Delta << \tau \quad (2.21)$$

Therefore if Δ is much smaller than the time constant of the system, $f(t)$ can be assumed as an impulse for the system.

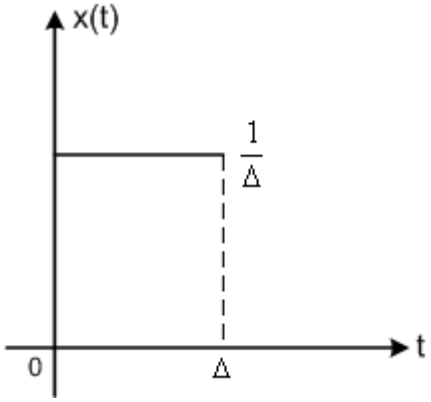

Figure 2.5 A typical input for the system.

The next question is that how small Δ should be in order to consider $f(t)$ as an impulse for the system. To answer this question all the terms of the equation 2.19, but the first

two ones are assumed to be zero. It is assumed that the second term can be ignored if it is smaller than 10% of the total value, which means:

$$Y(s) = \frac{\tau}{1+\tau.s} - \frac{\tau}{2!} \times (\frac{\Delta.s}{1+\tau.s}) \quad \xrightarrow{L^{-1}} \quad y(t) = \tau.e^{-\tau.t} - \frac{\tau.\Delta}{2!}(-\tau.e^{-\tau.t}) \tag{2.22}$$

$$\tau.e^{-\tau.t} < 10\% \times (\tau.e^{-\tau.t} - \frac{\tau.\Delta}{2!}(-\tau.e^{-\tau.t})) \tag{2.23}$$

$$1 < 0.1 \times (1 + \frac{\tau.\Delta}{2}) \tag{2.24}$$

$$20 < 2 + \tau.\Delta \tag{2.25}$$

$$18 < \tau.\Delta \tag{2.26}$$

Therefore, in order to ignore the second term of the equation 2.22, not only Δ should be much smaller that the time constant ($\Delta << \tau$), but also the equation 2.26 should be considered. The same method can be generalized to other terms of the equation.

It must be noted that the impulse response of a battery is related to various parameters such as state-of-charge, state-of-health, temperature and the magnitude of the current applied to the battery to calculate the impulse response. Different battery states result in various impulse responses corresponding to that specific situation.

2.3 Simulation and Experimental Results

As mentioned earlier, the impulse response of a battery can be used as a model to investigate the electrical and dynamic behavior of the battery. To validate this idea two different types of Li-Ion batteries, 18650 and 26650 have been used for experimental tests. The capacity of the 18650 battery is 2.2Ah and the capacity of the 26650 battery is 3.0Ah. The experiments have been done in room temperature, $25\,^{o}C$. The idea has been verified by simulation results using Battery Design Studio software V13.6 and the model of 18650 Li-Ion battery. Figure 2.6 shows the impulse response of the 18650 Li-Ion battery model for state-of-charge of 80% and Figure 2.7 shows voltage responses of the same battery model to various current magnitudes of 0.5A, 1A and 1.5A while SOC is equal to 80%.

To identify the impulse response of the battery, a specific discharging pulse is applied to the battery with a known state-of-charge. The measured voltage waveform along with the applied current is used by the System Identification Toolbox from MATLAB® to calculate the impulse response. Using this toolbox, the impulse response is identified and stored in the form of ARMAX model. The identified impulse response can be used as the battery model to calculate the output voltage of the battery.

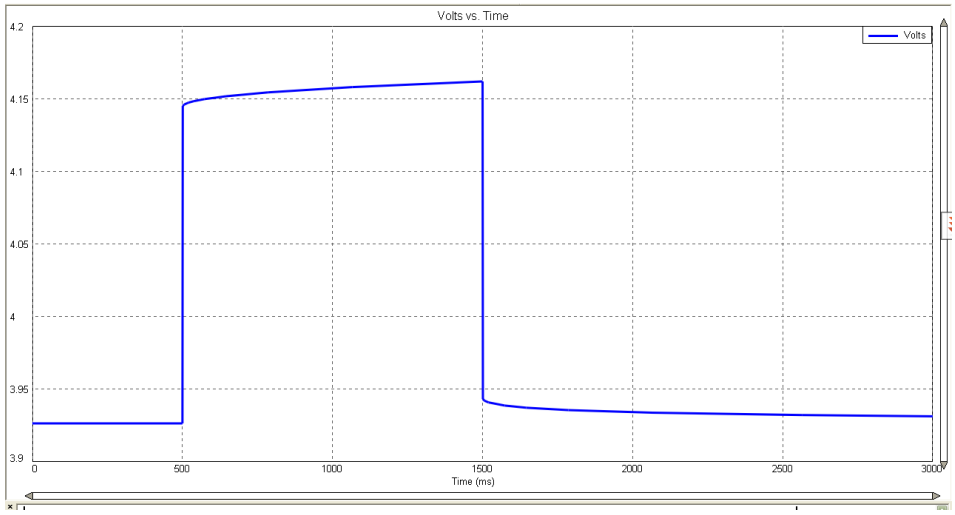

Figure 2.6 Impulse response of 18650 Li-Ion battery, SOC = 80%.

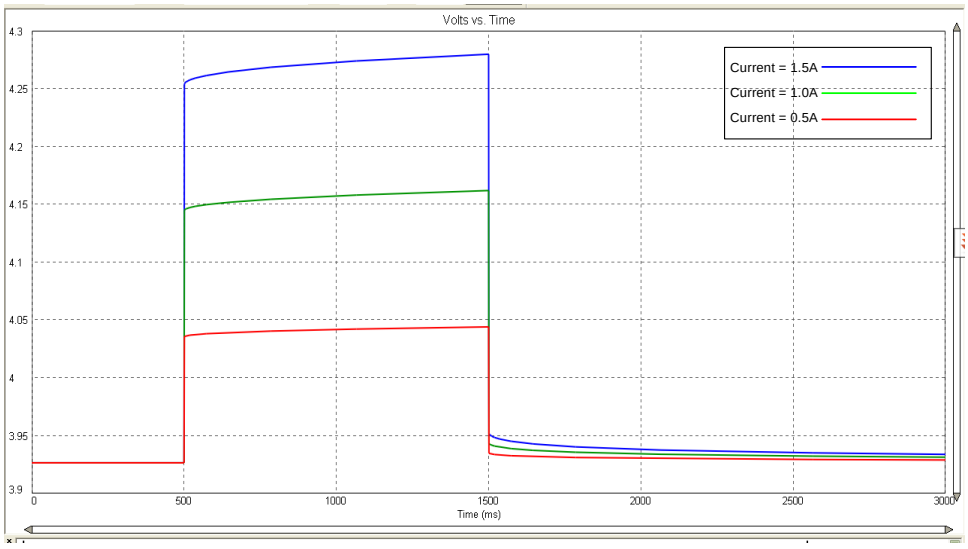

Figure 2.7 Charging pulse of 1s for different current magnitudes 0.5A, 1A and 1.5A, SOC=80%.

Figure 2.8 compares the measured voltage from terminals of the 18650 Li-Ion battery with the calculated voltage using impulse response of the cell. Two charging current pulses with the magnitude of about 1A and various lengths have been applied to the battery and also are used to calculate the output voltage using the battery impulse response. It can be observed that the error between the calculated and the measured voltages is less than 0.5%.

The same comparison has been accomplished for the 26650 Li-Ion battery in Figure 2.9 and Figure 2.10. In Figure 2.9, a discharging current pulse of about 2.5A is applied to the battery and the measured voltage is compared to the result of convolving the same current waveform with the impulse response of the battery. It is shown that the percentage of the fitness between measured and calculated voltages is 89%. Figure 2.10 depicts the same comparison for two discharging current pulses. The fitness in this figure is about 91%.

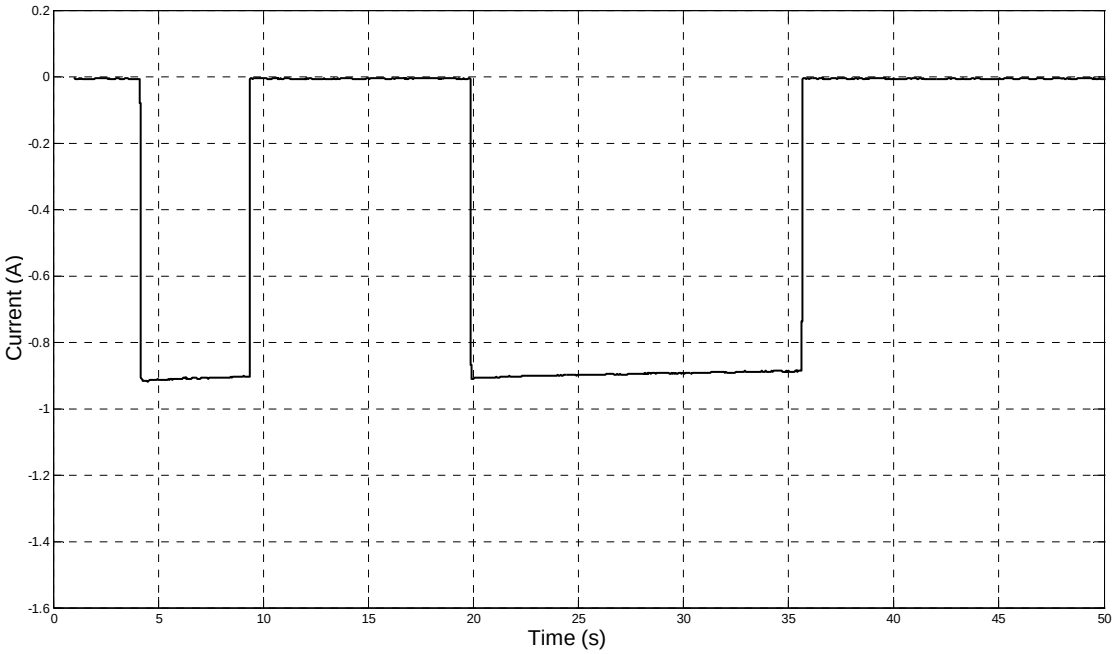

(a)

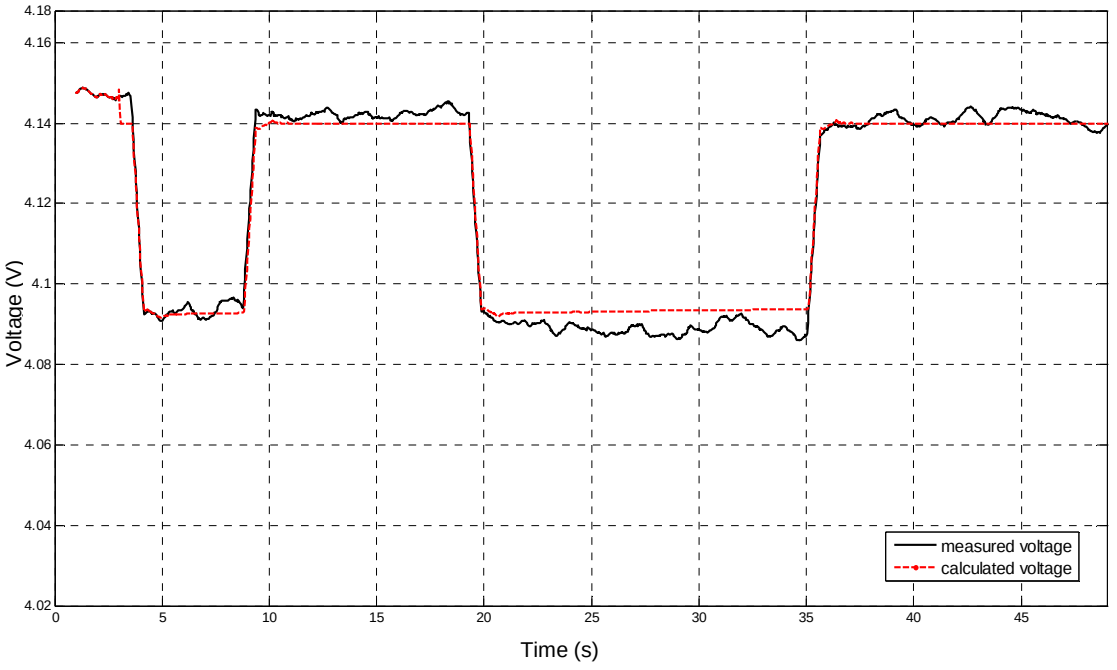

(b)

Figure 2.8 Comparison between measured and calculated voltages using the battery impulse response for 18650 Li-Ion battery, SOC = 100%. (a) applied current and (b) output voltages.

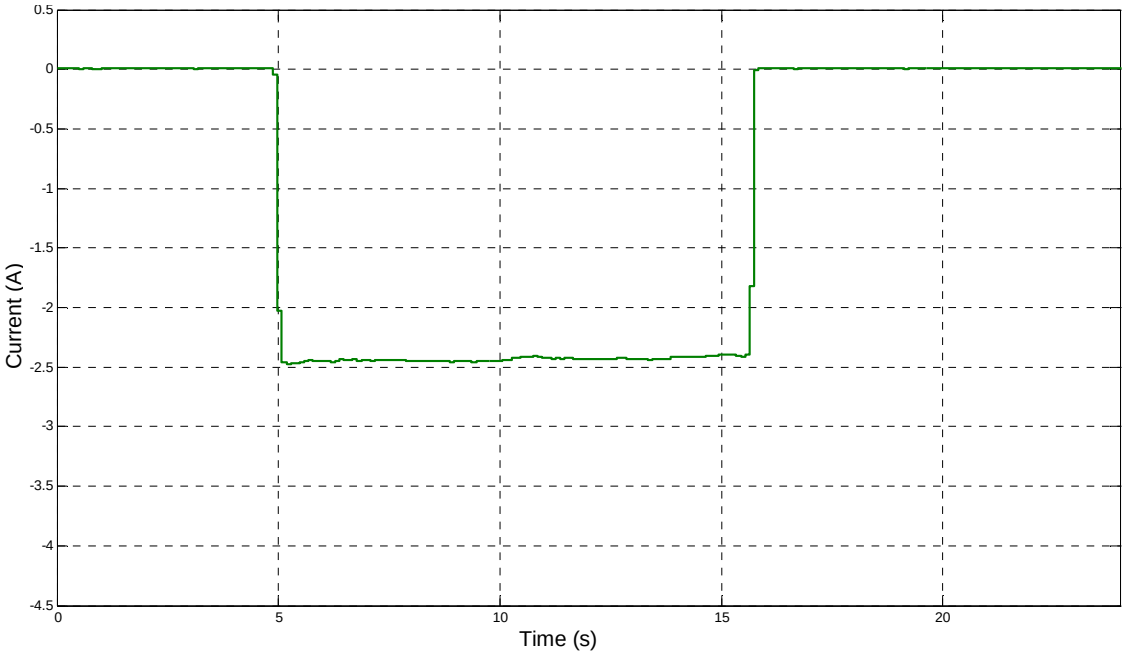

(a)

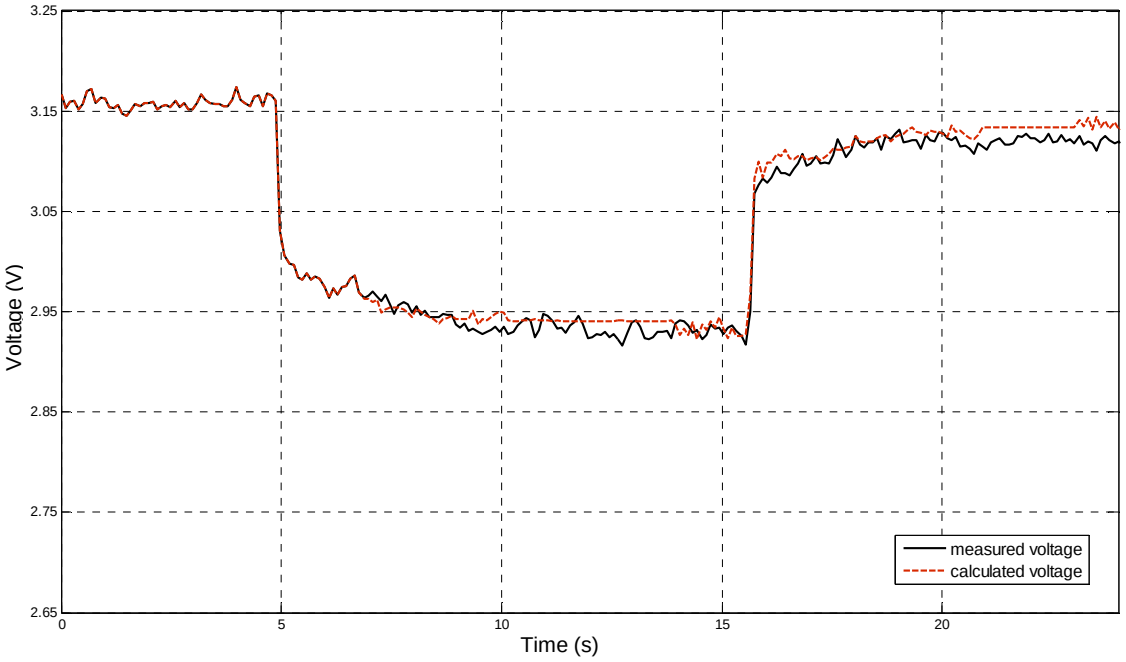

(b)

Figure 2.9 Comparison between measured and calculated voltages using the battery impulse response for 26650 Li-Ion battery for one discharging pulse, SOC = 90%. (a) applied current and (b) output voltages.

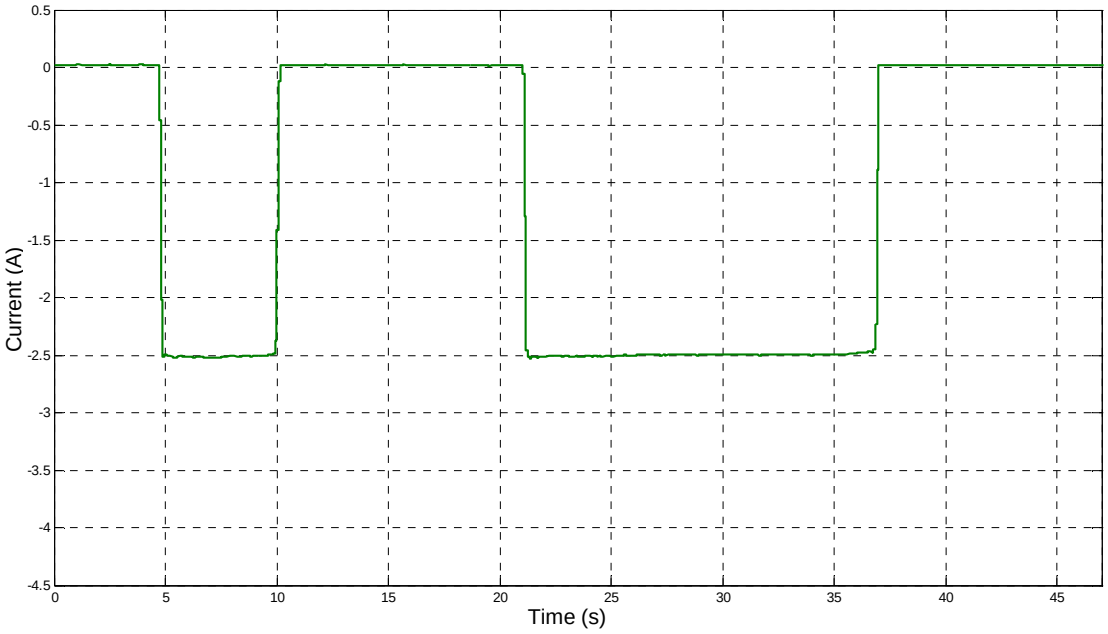

(a)

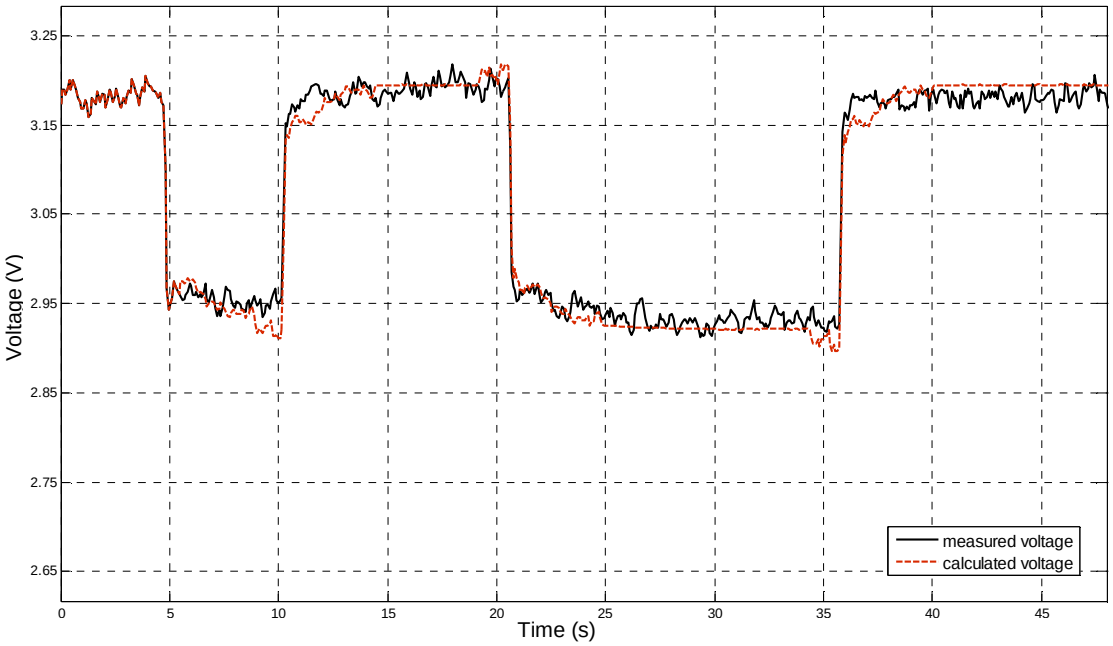

(b)

Figure 2.10 Comparison between measured and calculated voltages using the battery impulse response for 26650 Li-Ion battery for two discharging pulses, SOC = 100%. (a) applied current and (b) output voltages.

CHAPTER 3

STATE-OF-HEALTH ESTIMATION USING IMPULSE RESPONSE

This chapter describes various possible fault can occur inside the battery and parameters contributing to the battery aging. A novel method based on the impulse response of the battery for estimating the battery state-of-health is introduced here. The proposed method is validated by simulation and experimental results.

3.1 Fault classification

Li-Ion batteries have specific characteristics such as high power and energy density in comparison to other conventional batteries which make them possible to be reduced in the size and weight and hence improving this technology for Electric and Hybrid Electric Vehicles (EV/HEV). However, life time performance remains an issue for Li-Ion batteries. Identifying the causes of battery degradation and investigating the impact of different accelerating factors on the specific degradation and as a result on the life time of the battery have been an ongoing challenge in recent researches.

There are various parameters contributing to the battery aging process in Li-Ion batteries and they can be modeled in different ways. The most common parameters are addressed here.

3.1.1 Electrolyte decomposition

As mentioned in Chapter 1, the electrolyte consists of lithium salts dissolved in a solvent such as $LiPF_6$, $LiBF_6$ or $LiClO_4$ to act as a carrier, conducting lithium ions between anode and cathode. Considering $LiPF_6$ as active material of the electrolyte, the following reaction takes place:

$$LiPF_6 \Leftrightarrow LiF + PF_5 \tag{3.1}$$

PF_5 reacts readily with the solvents to form decomposition products on the surface of the electrode even at relatively low temperature (45^{o}C). The accumulation of the electrolyte decomposition products on the surface of the cathode particles causes active material isolation and an increase in the impedance at the cathode/electrolyte interface, resulting in the loss of capacity and power capability. Operating temperature of the battery has a significant impact over the film growth. The cycle life of a battery decreases as temperature increases.

In order to model the electrolyte decomposition by software, the electrolyte density of the battery can be decreased. Another method for modeling this fault is to reduce the available active area over positive electrode by minimizing the cathode width.

3.1.2 Formation of surface films on positive electrode

The positive electrode is generally composed of a lithium metal oxide such as $LiCoO_2$, $LiNiO_2$ and $LiMn_2O_2$. The negative electrode is a carbon-based material which is normally made of graphite. The decomposition of the $LiCoO_2$ as the active material of positive electrode may be presented as follows:

$$LiCoO_2 \rightarrow (1-x)[Co_3O_4 + O_2 \uparrow]/3 + xLiCoO_2 \tag{3.2}$$

where the active material decomposes into inactive Co_3O_4, which will be formed at the surface of the cathode. This phenomenon reduces the amount of active material available in the positive electrode. It means that the amount of electrochemically active Li^+ ions that can interact in the cathode or on the other hand the maximum capacity of the positive electrode (Q^+_{max}) will decrease. As a result, the EMF model parameters of the battery (from Figure 1.4) will also change. Figure 3.1 shows the schematic representation of aged battery parameters which is characterized by a similar set of parameters as in Figure 1.4. In order to compare both models, the parameters related to the healthy battery are also represented here.

Because of the Co_3O_4 layer formation over the positive electrode surface, an amount of active Li^+ ions remains stored inside the electrode. This is the reason that the overall amount of Li^+ ions inside the aged battery Q_{amax} is higher than the maximum capacity of the positive

electrode Q^{+}_{amax}, whereas in a healthy battery, Q^{+}_{max} is higher than Q_{max}. By aging the battery, the amount of Li^{+} ions which remains inside the negative electrode at the end of discharge (Q^{-}_{a0} comparing to Q^{-}_{0}) will also increase.

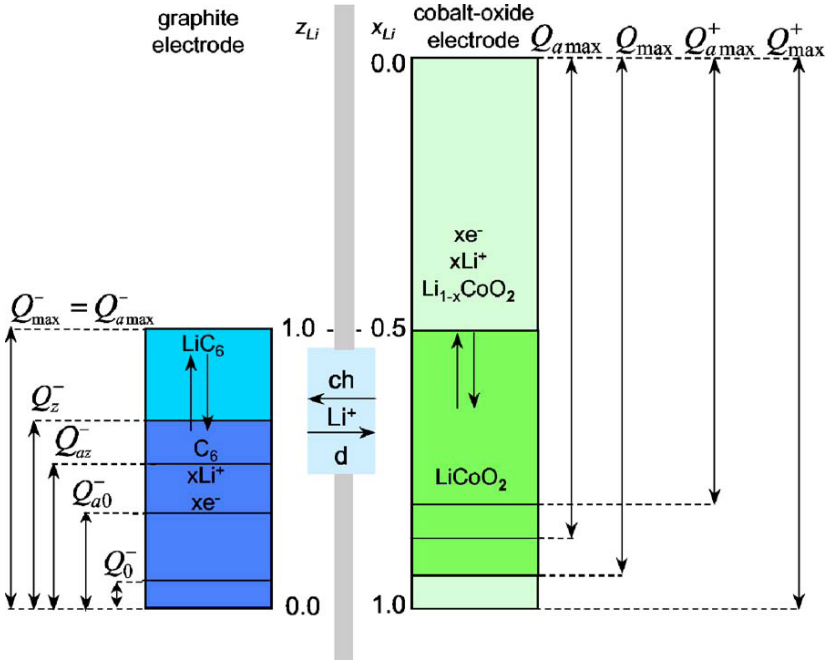

Figure 3.1 Schematic representation of an aged Li-Ion battery (courtesy of [6]).

Formation of particles at the electrode surface also causes an increase of the battery impedance. A battery with low cathode capacity might still be able to deliver an acceptable charge for low discharge C-rate currents, but it cannot perform properly at higher C-rate currents.

Software modeling of the positive electrode decomposition can be done by reducing the active material density in the cathode. In this way, the total amount of Li^{+} ions available decreases and the overall storage capacity of the battery will decrease.

3.1.3 Internal short circuit (soft short)

A Li-Ion battery is made of coated anode and cathode separated by thin layers of polymer material called separator. The width of the separator is normally less than 25 um and

the thinner this layer is made more energy density in smaller volume of battery is achieved. If the battery is used in high temperature the separator may be melted in some points and punctured. It also can happen if some manufacturing faults occur during creating individual cells or when the battery is under pressure in specific situations.

By puncturing the separator anode and cathode of the battery will be shorted and a current path is created between two electrodes which causes the battery to discharge internally. The self-discharge of the battery because of internal short circuit which is called “soft short” is one of the factors causing battery temperature to rise and it disables battery to hold its charge naturally, hence it deteriorates the health status of the battery. In the worst case, it could leads to thermal runaway and causes ignition or explosion of the cell. Accidents involving Li-Ion batteries have occurred frequently [41].

There have been numerous instances of the Li-Ion batteries used in laptop computers or cellular phones overheating or catching fire. The cause of these faults is assumed to be an internal short circuit which is one of the factors increasing the battery temperature. Figure 3.2 shows a simple circuit model to demonstrate the heat generations when an external or internal short circuit occurs [42].

For the case of external short circuit, W_i generated by short circuit current I in internal resistance R_i is calculated as follows:

$$W_i = \int_{-\infty}^{+\infty} I^2 R_i .dt \tag{3.2}$$

$$I = E/(R_i + R_s) \tag{3.3}$$

$$W_i = \int_{-\infty}^{+\infty} E^2 R_i /(R_i + R_s)^2 .dt \tag{3.4}$$

W_i has the highest value when the short-circuit resistance $R_s = 0$ and it decreases as R_s increases. External short circuits can be prevented with electric protection circuits.

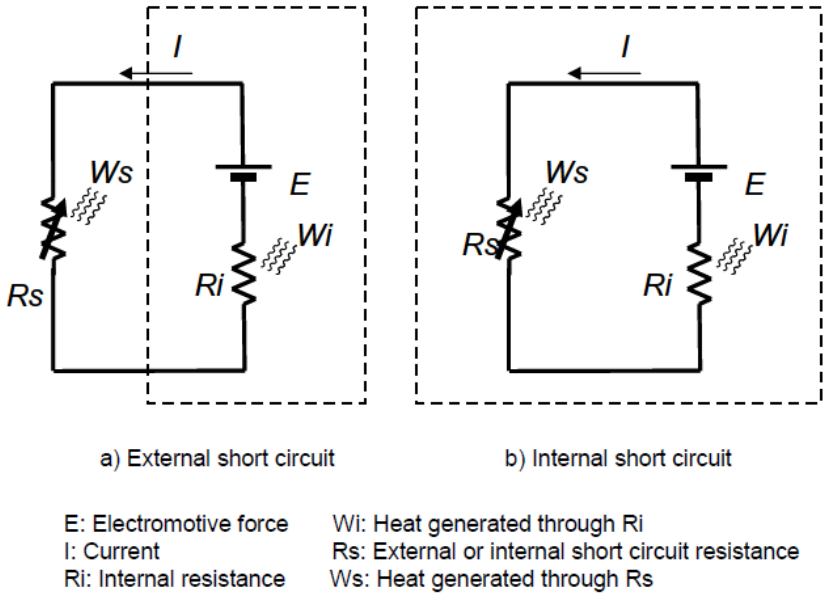

Figure 3.2 Simple equivalent circuit model for a shorted battery (courtesy of [42]).

In the case of internal short circuit, the model is the same as the one for the external short circuit except that both short circuit resistance R_s and internal resistance R_i are inside the battery. The heat generated by the short circuit resistance R_s causes local and rapid heating inside the battery. The heat W_s generated by short circuit current I inside the internal short circuit resistance R_s is calculated by the following equations:

$$W_s = \int_{-\infty}^{+\infty} I^2 R_s .dt \tag{3.5}$$

$$I = E/(R_i + R_s) \tag{3.6}$$

$$W_s = \int_{-\infty}^{+\infty} E^2 R_s /(R_i + R_s)^2 .dt \tag{3.7}$$

W_s has the highest value when the short circuit resistance R_s is the same value as the internal resistance R_i which is the most dangerous condition. The internal short circuit cannot be protected using an external protection circuit and it is one of the worst scenarios in battery technology which there is nothing that can be done for that.

To know the tolerance of the Li-Ion batteries to internal short circuit, several tests need

to be done. One popular test is the nail penetration test which simulates the situation of the internal short circuit inside a battery and the response of the cell to such failure is investigated. In this test a narrow iron nail penetrates into the battery and creates a multi-point internal anode to cathode short. Response of the battery is monitored using a high speed camera. There are many parameters to consider in a nail test, such as the nail size and penetration speed and the leakage of accumulated gas and electrolyte from pierced point [42-43].

Another method to study the internal short circuit is the crush test. This method simulates a massive internal short circuit of a cell by crushing the cell. Special tools are used for this purpose in order to assure maximum internal damage without cracking the case. The crush test has some advantages comparing to the nail test, for example there is no leakage of the electrolyte because there is no hole over the cell case, and as a result the internal short circuit situation is modeled more precisely [43].

3.2 Fault Simulation and Analysis

To study the effect of various faults over the battery behavior, different faults have been simulated using Battery Design Studio software V13.6 and the model of 18650 Li-Ion battery with the capacity of 2.2Ah. This software is designed for data analysis, design and simulation of the batteries. Various parameters of the battery can be specified by the user and their effect on the battery behavior can be studied.

Both electrolyte and electrode decompositions lead to formation of a layer over positive electrode and reduction of its active area. Figure 3.3 shows the effect of reducing cathode active area on the voltage response of the battery. A charging current of 1A is applied to the 18650 Li-Ion battery software model with the SOC of 70%. It is shown that the output voltage response varies regarding to the amount of active area reduction.

Another method to model the electrolyte decomposition is to reduce the electrolyte density. Figure 3.4 shows the effect of electrolyte decomposition by decreasing the electrolyte

density of the battery with various rates of 30%, 40% and 50%. It is shown that various results are achieved regarding different electrolyte densities.

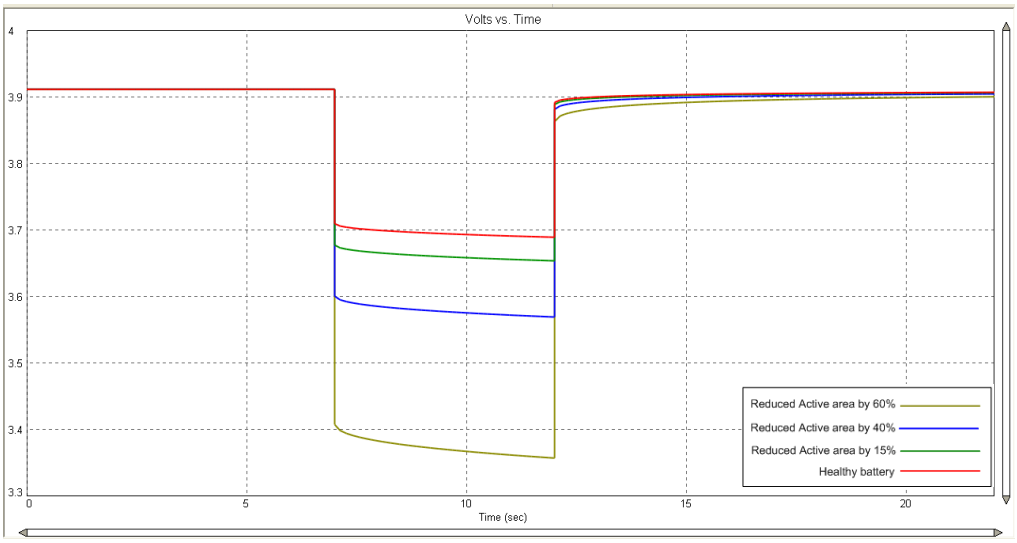

Figure 3.3 The effect of reducing cathode active area on voltage response to discharging current pulse of 1A for 1s, SOC = 70%.

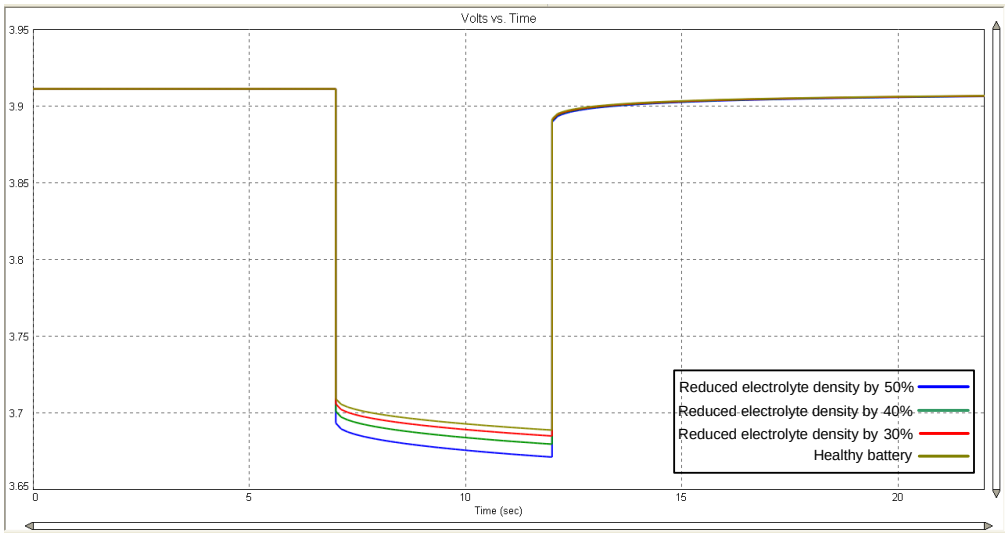

Figure 3.4 The effect of electrolyte density reduction on voltage response to discharging current pulse of 1A for 1s, SOC = 70%.

As it is shown in Figure 3.3 and Figure 3.4 the battery sensitivity to the electrolyte decomposition is less than its sensitivity to the positive electrode decomposition. In other words the voltage response of the cell changes dramatically when the active area reduces, but

changing in the electrolyte density does not make a significant difference in the output voltage. Small changes in the voltage could be caused by several possible situations, for example, reduced active area by 15% leads almost to the same situation as the reduced electrolyte density by 50% (Figure 3.3 and Figure 3.4).

The mentioned phenomenon can be used as a signature to distinguish between these two types of faults. Because of the higher sensitivity of the battery voltage response to the active area reduction comparing to the electrolyte density decrease, the response of the battery to larger current magnitudes would encounter more changes as well. Figure 3.5 compares the two different cases which make close changes in the voltage response of the battery: electrolyte density reduction by 50% and active area reduction of the positive electrode by 15%. The figure shows how increasing the current magnitude applied to the battery will increase the effect of the active area reduction of the positive electrode more than the effect of the electrolyte density reduction.

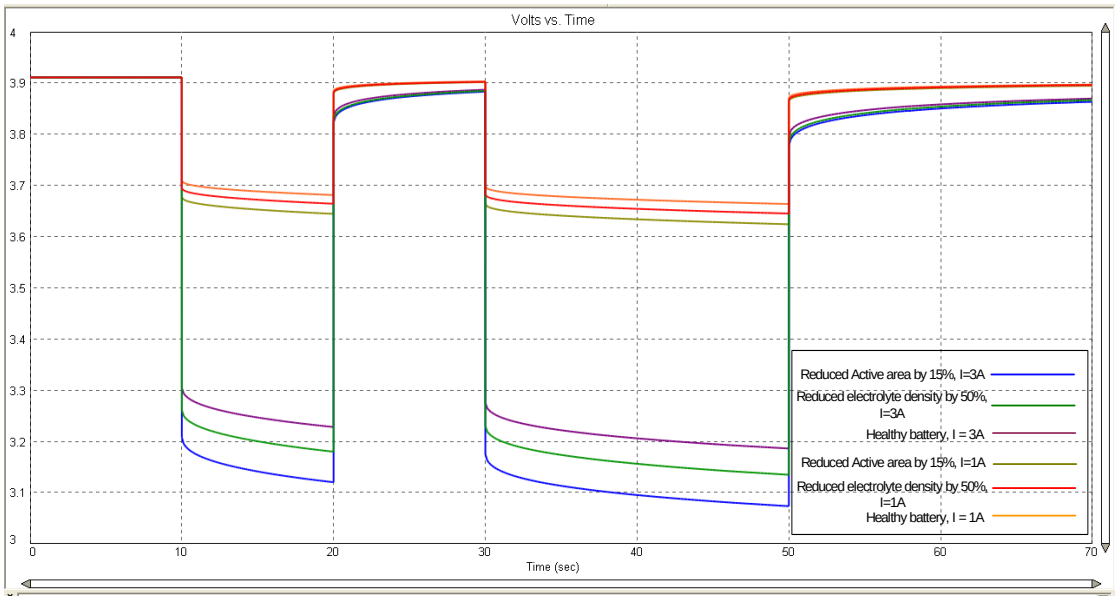

Figure 3.5 The effect of change in current magnitude on the voltage response for two different fault situations.

3.3 State-of-health Estimation Method

In this section the proposed method for estimating the SOH of Li-Ion batteries is explained. For modeling the battery in the proposed method, the impulse response of the battery introduced in chapter 2 is applied. The impulse response is dependent upon the amount of charge left in the battery (SOC) and also the health status of the battery (SOH). Different levels of SOC and various faults imply different impulse responses. It must be noted that the term impulse inherently suggests that the duration of the current pulse is significantly smaller than the smallest time constant in the system.

3.3.1 Method description

Figure 3.6 shows the block diagram of the SOH estimation algorithm. A family of impulse responses for various levels of SOC for a healthy battery are recorded and used such that the whole available range of the SOC of the battery is being presented by "n" individual values corresponding to a specific impulse response ($h_n[k]$). The impulse responses corresponding to different SOCs are formatted into an ARMAX model and the corresponding coefficients are stored in a look-up table. As mentioned previously the multivariable ARMAX model is shown as:

$$A_0 \times y(t) + A_1 \times y(t-T) + \ldots\ldots + A_n \times y(t-nT) = B_0 \times u(t) + B_1 \times u(t-T) + \ldots\ldots + B_m \times u(t-mT) + e(t) \quad (3.8)$$

The coefficients would be determined based on the current and voltage input waveforms used for impulse response calculation. Using the experimental data, the impulse response of the battery is represented as follows:

$$y(t) = B_0 \times u(t) + B_1 \times u(t-T) + \ldots\ldots + B_m \times u(t-mT) + e(t) \quad (3.9)$$

Measuring the SOC of the battery using SOC estimator block, the impulse response of the battery corresponding to the specific SOC is selected and used for convolution by the arbitrary input current to calculate the output voltage.

The impulse responses corresponding to different fault situations are also stored in a look up table. The applied current to the battery is convolved with all these impulse responses and a set of output voltages are calculated. The measured output voltage from terminals of the battery and the calculated output voltage using the specific impulse response corresponding to the battery state-of-charge are compared using the fitness function explained in section 3.3.2 to determine the health condition, possible fault occurred and the lifetime of the battery [44].

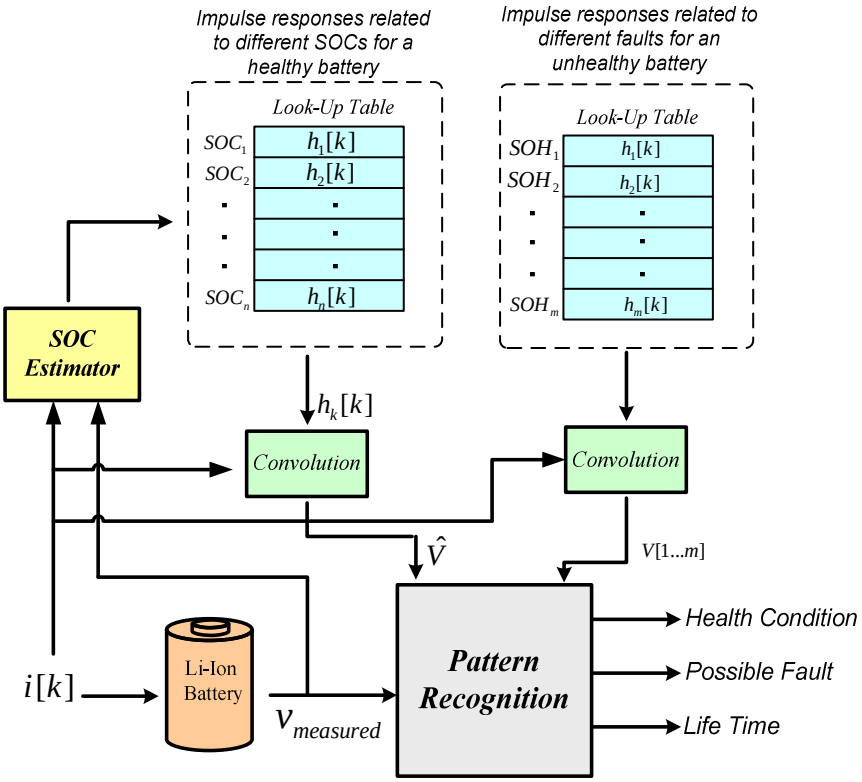

Figure 3.6 The state-of-health estimation algorithm.

The pattern recognition block itself contains of two different comparison blocks. After the first comparison of the voltage waveforms using the fitness function another comparison is made for the waveforms with close fitness percentages, but this time by applying a larger current magnitude to the cell. Because of the higher sensitivity of the battery voltage to one type of fault comparing to the other type, the exact type of the fault and the health condition of the

cell is determined using this method. The life time of the battery is also estimated by the comparison of the fitness percentage of the healthy battery impulse response with the best fit to the measured voltage. Figure 3.7 depicts the details of the pattern recognition block.

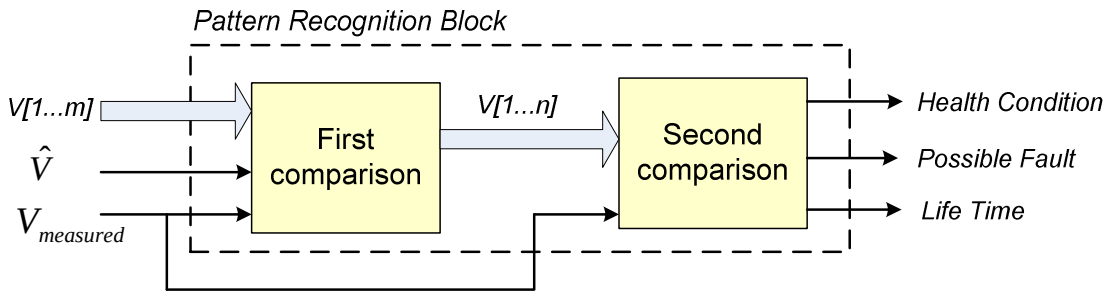

Figure 3.7 The pattern recognition block in detail.

3.3.2 Comparison method

In order to compare the calculated voltage waveforms with the measured voltage of the battery in pattern recognition block, a mathematical method is used. This method calculates the percentage of the output that the impulse response model reproduces which is called the Fitness percentage. The Fitness (%) is based on the mean square error between the measured data and the simulated output of the model which is calculated as follows:

$$E = \frac{1}{n}\sum_{i=1}^{n}\left(\frac{V_i - \hat{V}_i}{V_i}\right)^2 \tag{3.10}$$

$$Fit(\%) = (1-E)\times 100 \tag{3.11}$$

where V_i and $\hat{V}_i$ are the measured and calculated data samples and n is the number of the samples. 100% corresponds to a perfect fit (no error) and 0% corresponds to a model which is not capable of estimating any variation of the output. By calculating the Fitness value of a battery model the accuracy of the model in estimating the response of the battery is verified and by comparing the Fitness values of various models, the model with the best fit for the battery is identified.

The amount of the Fitness percentage depends on the specific variables such as state-of-charge, temperature and the current magnitude. Based on the variations in these variables the amount of the Fitness would change. The sensitivity of the Fitness function is defined as follows:

$$S^{Fit} = \frac{\partial Fit}{\partial SOC} + \frac{\partial Fit}{\partial T} + \frac{\partial Fit}{\partial I} \tag{3.12}$$

The measured voltage of the battery (V_i) used in Equation 3.10 is related to the open-circuit voltage (EMF) and the current magnitude by the following equation:

$$V_i = EMF - RI(t) \tag{3.13}$$

where R is the internal resistance of the battery. The EMF-SOC relationship is verified in section 1.2.3 (equations 1.3, 1.4 and 1.6) which also depicts the dependency of the EMF to the temperature. Having all these equations the dependency of the Fitness function to the SOC, temperature and current of the battery is verified.

3.3.3 Simulation results

To verify the proposed method by simulation six different fault situations are selected which are as follows:

- active area reduction of the positive electrode by 15%
- active area reduction of the positive electrode by 40%
- active area reduction of the positive electrode by 60%
- electrolyte density reduction by 30%
- electrolyte density reduction by 50%
- electrolyte density reduction by 70%

The impulse responses corresponding to these faults for a specific state-of-charge (SOC = 70%) are calculated and stored in the form of ARMAX model. The System Identification Toolbox

from MATLAB® is used to calculate the required impulse responses. The impulse response of the healthy battery for SOC of 70% is also calculated and stored.

A discharging current pulse with the magnitude of 1A is applied to the 18650 battery model of the Battery Design Studio software. The same current waveform is applied to all impulse responses and the calculated voltages along with the measured voltage are compared using the fitness function explained in section 3.3.2. If there is one waveform which fits the measured voltage the best and its fitness percentage is significantly higher than the values of other waveforms, then the decision about the health status and the possible fault can be made at this time. But if the fitness percentages for some of the waveforms are close and a certain decision cannot be made, then the second level of comparison is implemented. In this level the current magnitude is increased to 3A in order to verify the sensitivity of the remained impulse responses and find the best fit.

Figure 3.8 shows the case that the battery has the fault of reduced active area of the positive electrode by 40%. The current waveform of Figure 3.8(a) is applied to the battery and also is convolved by the impulse responses to calculate the output voltages. All the measured and calculated voltages along with their fitness percentages are shown in Figure 3.8(b). As it is shown in the figure the calculated voltage using the impulse response corresponding to the reduced active area by 40% has the best fit to the measured voltage and because its fitness percentage has a significant different with the other fitness values, the second level of comparison is not necessary. Figure 3.9 shows the same case as Figure 3.8 but this time for one discharging pulse of current with the length of 12s.

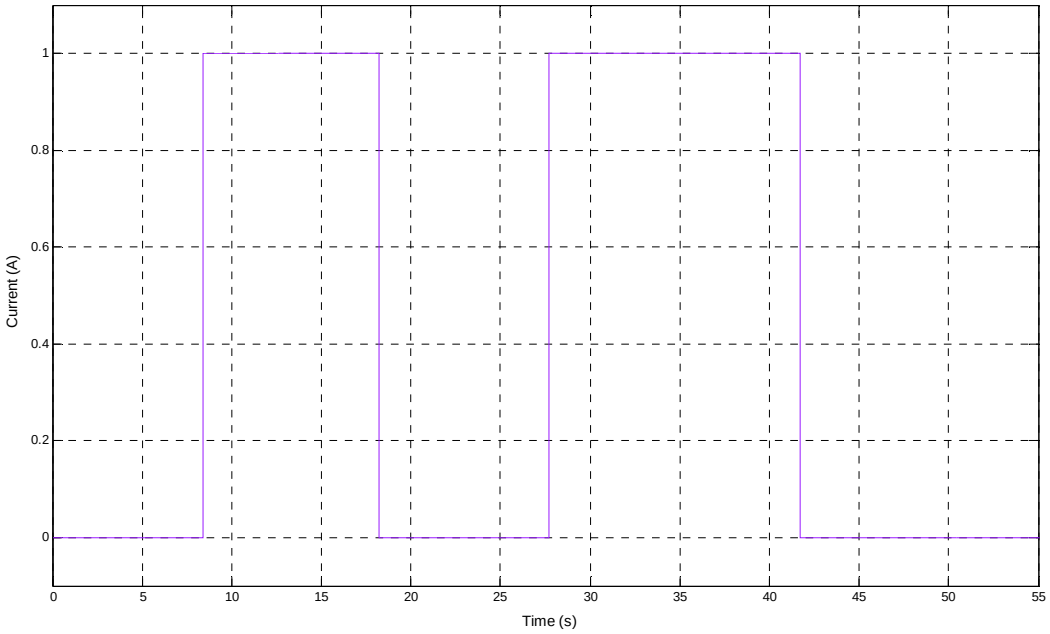

(a)

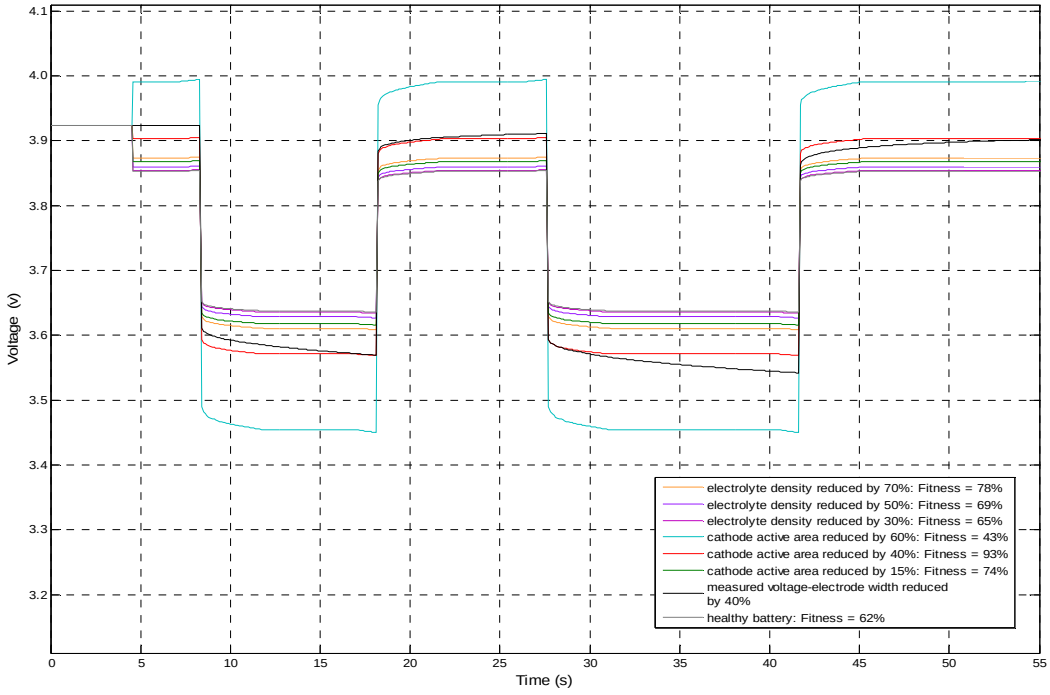

(b)

Figure 3.8 Method validation for the battery with the fault of reduced active area of the positive electrode by 40% for two discharging current pulses. (a) applied current waveform and (b) comparison of measured and calculated voltages.

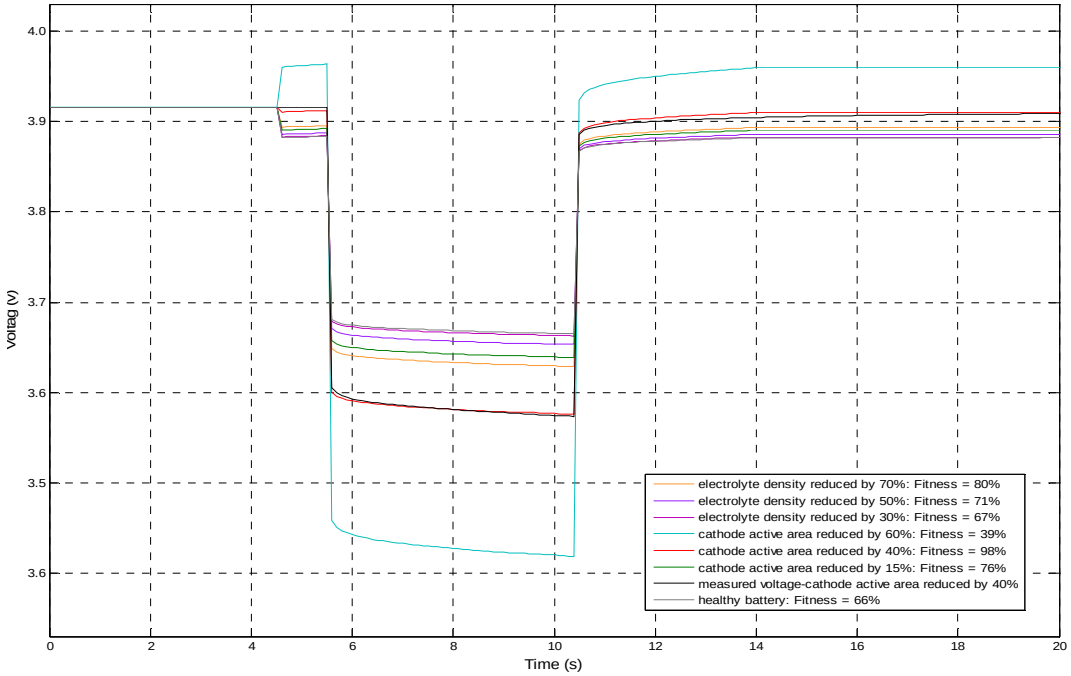

Figure 3.9 Method validation for the battery with the fault of reduced active area of the positive electrode by 40% for one discharging current pulse.

Figure 3.10 shows the case that the battery has the fault of electrolyte density reduction by 70%. As it is shown in Figure 3.9(a) the fitness value for the waveform corresponding to the reduced electrolyte density by 70% is close to the one related to the reduced active area by15% and the one corresponding to the reduced electrolyte density by 50%. For this reason next level of comparison needs to be run on the impulse responses with close fitness values. Figure 3.9(b) shows the second comparison by applying the same current waveform as Figure 3.8(a) but with the magnitude of 3A. The fitness value for the waveform corresponding to reduced electrolyte density by 70% is higher comparing to the other two values and it is introduced as the fault occurred inside the battery.

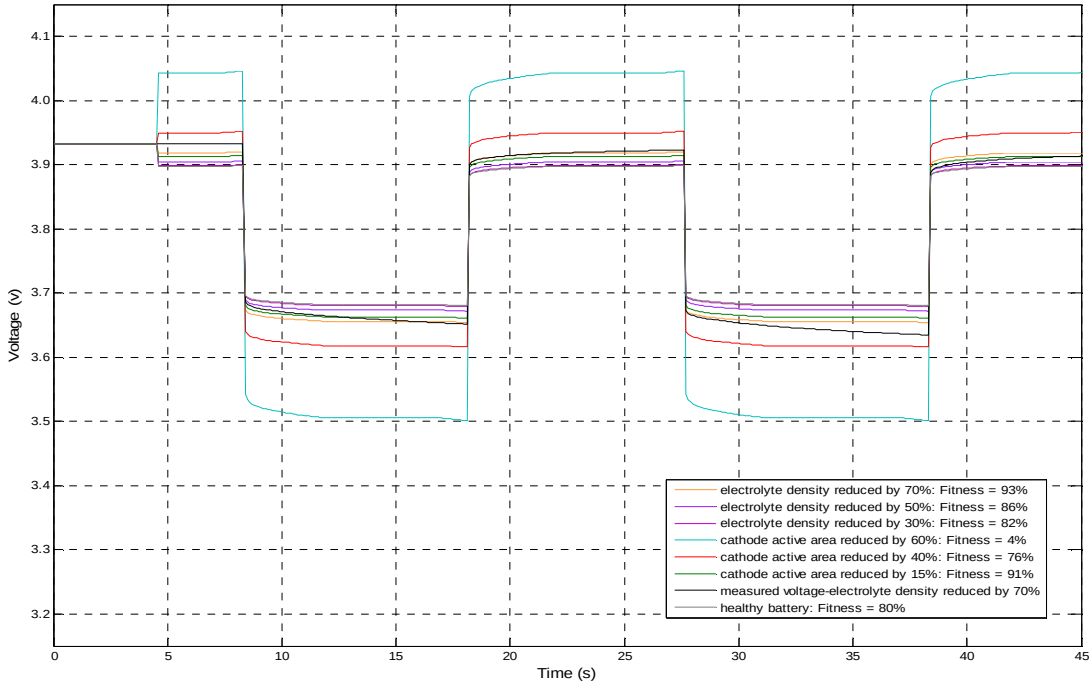

(a)

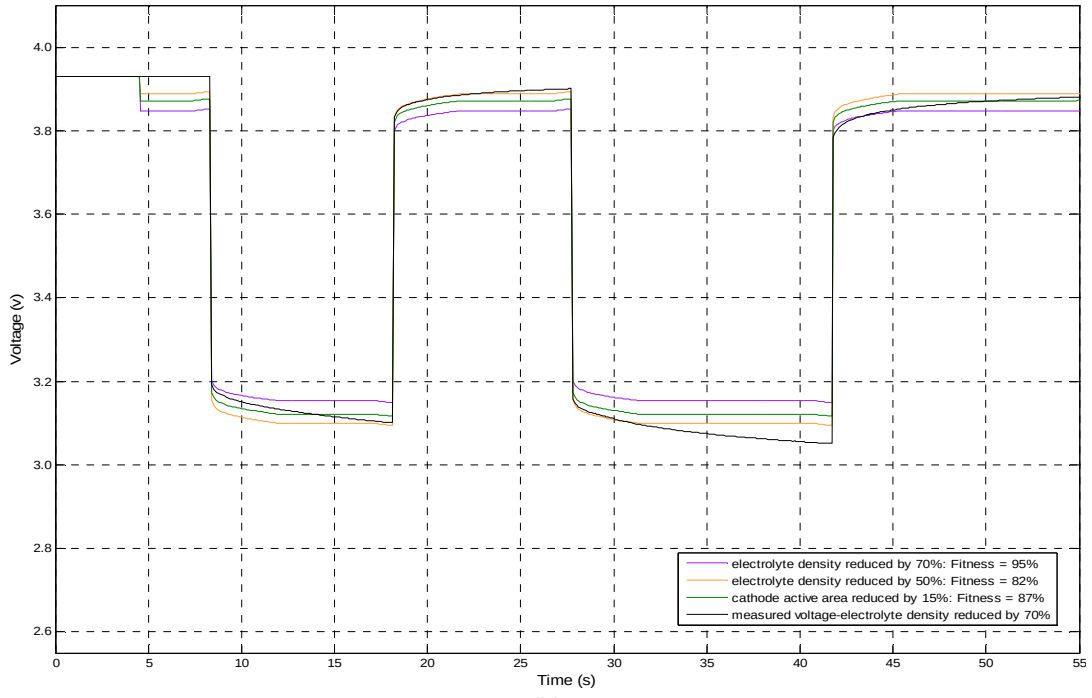

(b)

Figure 3.10 Method validation for the battery with the fault of electrolyte density reduction by 70%. (a) first comparison and (b) second comparison.

3.3.4 Experimental results

A new 26650 Li-Ion battery has been used for experimental results. The capacity of the battery is 3.0Ah and the experiments have been done in room temperature, $25^{o}C$. Using a specific discharging pulse, the impulse response of the battery with a specific state-of-charge is identified and stored in the form of ARMAX model using the System Identification Toolbox from MATLAB®. The calculated impulse responses for various levels of SOC are used as the battery model to calculate the output voltage.

To verify the proposed method, a new (healthy) and an aged 26650 Li-Ion batteries are selected. The health status of the aged battery is determined by discharge test. The impulse responses corresponding to both batteries are calculated and stored in the form of ARMAX coefficients. Then, by applying any specific current waveform to these impulse responses the expected voltage is achieved.

Figure 3.11 shows the comparison of calculated output voltages for both healthy and faulty batteries. A specific current waveform is applied to the healthy battery, and then the same current waveform is applied to both impulse responses of the healthy and aged batteries. The calculated output voltages using impulse responses are compared to the measured voltage from terminals of the battery. It can be noted that the voltage calculated by the impulse response of the healthy battery fits the measured voltage better than the one calculated by the impulse response of the faulty battery. The test has been done for two various current waveforms, the first one has one discharging pulse of about 10 seconds (Figure 3.11(a)) and second one contains two discharging pulses of 5 and 15 seconds (Figure 3.11(b)).

The same comparison as Figure 3.11 is performed in Figure 3.12, this time for the faulty battery. As it is shown in this figure the voltage calculated by the impulse response of the faulty battery has better match to the measured voltage comparing to the calculated voltage of the healthy battery.

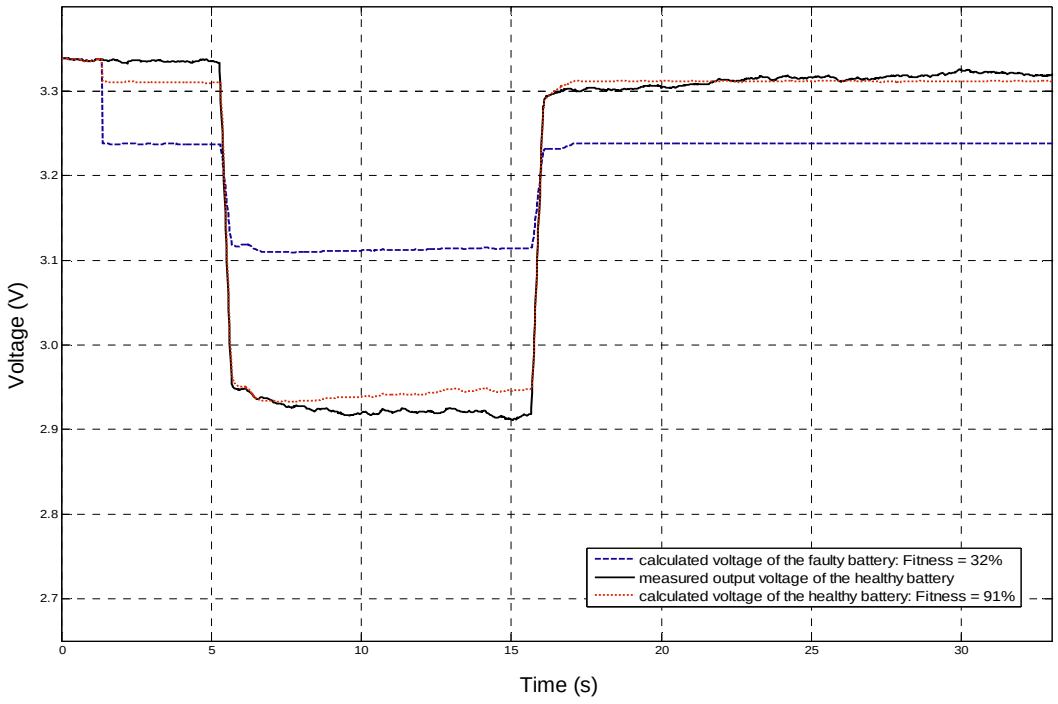

(a)

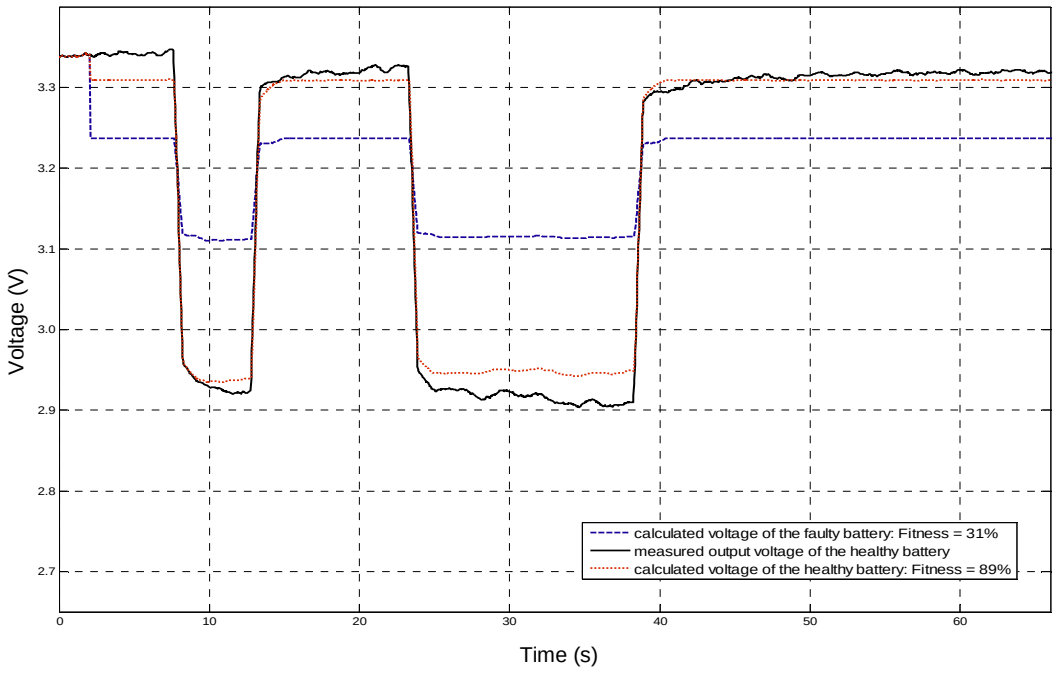

(b)

Figure 3.11 Comparison of the measured output voltage of the healthy battery and the calculated voltages of the faulty and healthy batteries, SOC = 100%. (a) voltage comparison for pulse length of 10s and (b) voltage comparison for two pulses.

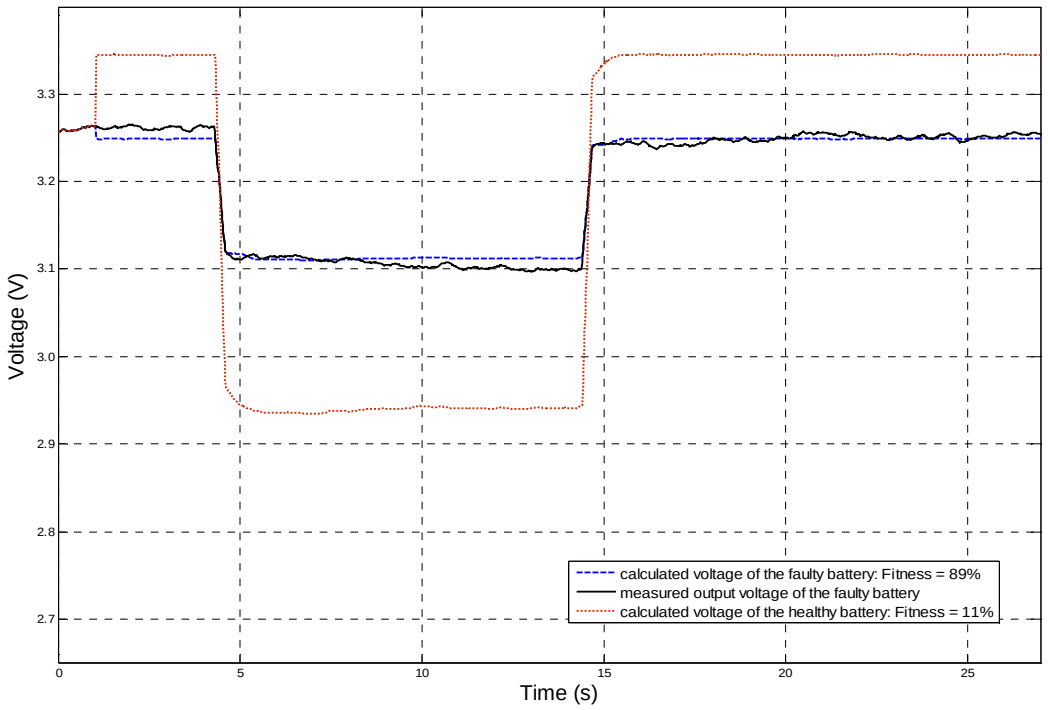

(a)

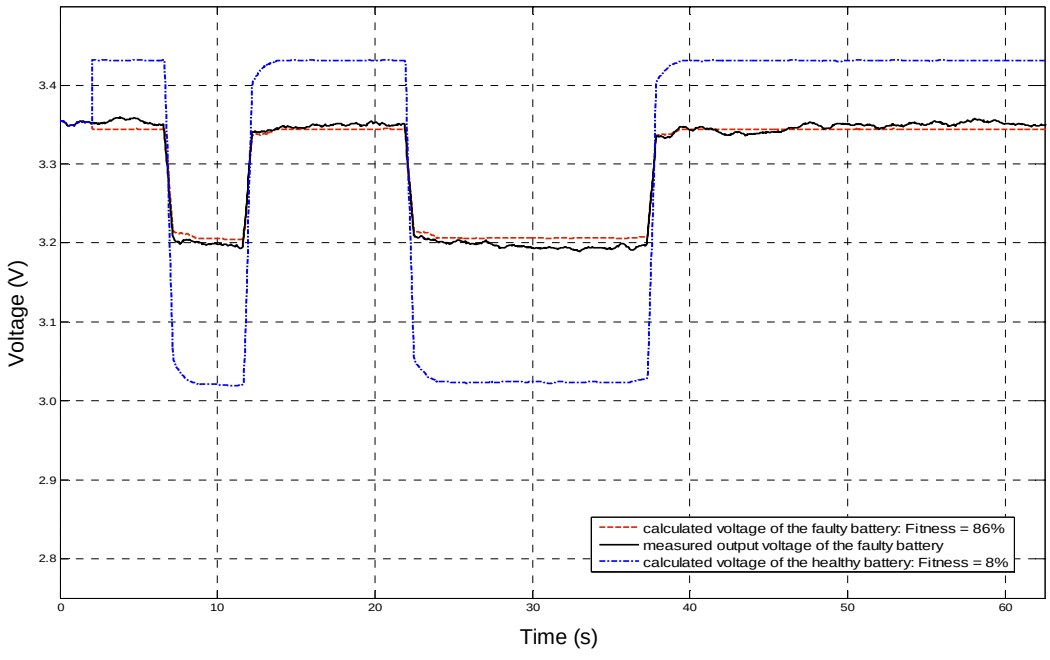

(b)

Figure 3.12 Comparison of the measured output voltage of the faulty battery and the calculated voltages of the faulty and healthy batteries, SOC = 100%. (a) voltage comparison for pulse length of 10s and (b) voltage comparison for two pulses.

CHAPTER 4

STATE-OF-CHARGE ESTIMATION USING IMPULSE RESPONSE

The present chapter introduces a novel method for estimating the state-of-charge of Li-Ion batteries based on their impulse response. A battery management system and an experimental test bed to validate the proposed method are developed.

4.1 Impulse Response Dependency on the State-of-charge

Any LTI system is completely characterized by its impulse response. The impulse response of an LTI system contains the main properties of the system. That means for any input function, the output function can be calculated in terms of the input function and the impulse response.

As mentioned in chapter 2, the impulse response of a battery is also dependent upon the main characteristics of the battery such as the magnitude of current, temperature, state-of-health. Another main property of the battery which effects on its impulse response is the amount of charge which is left in the battery or in other words its state-of-charge (SOC). Different levels of SOC imply different impulse responses. It must be noted that the term impulse inherently suggests that the duration of the current pulse is significantly smaller than the smallest time constant in the system.

The mentioned characteristic is verified by simulation and experimental results. For the simulation result, Battery Design Studio® V13.6 software has been used. A charging current pulse with magnitude of 1A and width of 1sec is applied to the 18650 Li-Ion battery model. This test has been done for a variety of state-of-charges and as it is shown in Figure 4.1 different responses are achieved.

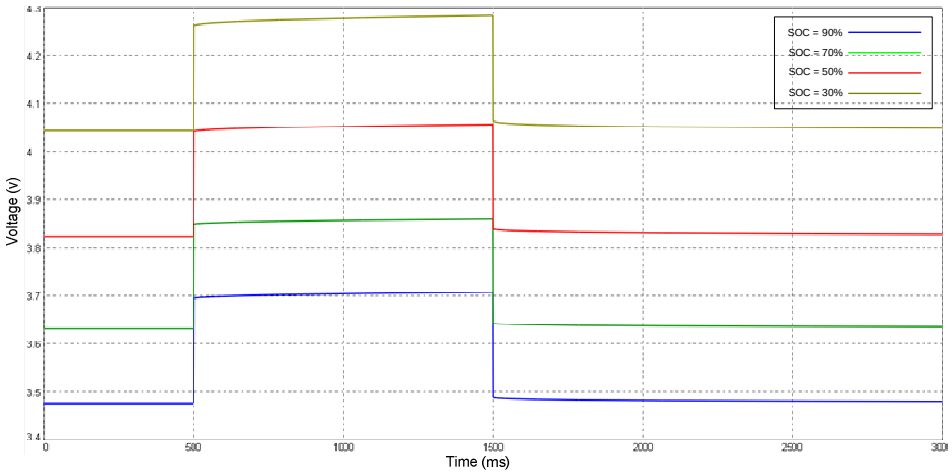

Figure 4.1 Comparison of the impulse responses for various SOCs 30%, 50%, 70% and 90%, for applying a charging current pulse of 1A.

To verify dependency of the impulse response of the battery to its state-of-charge experimentally, a 18650 Li-Ion battery is used. Figure 4.2 depicts different impulse responses of the experimental cell corresponding to state-of-charges of 75% and 20%. A narrow pulse of current is applied to the cell for various SOCs and as it is shown the resulting impulse responses are different for various levels of state-of-charge.

4.2 State-of-charge Estimation Method

The state-of-charge (SOC) estimation method proposed in this dissertation utilizes the battery impulse response concept in order to model the Li-Ion battery. The method models the battery using the impulse response method explained in chapter 2, then it uses the dependency of the battery impulse response to its state-of-charge and based on this relationship estimates the SOC of the cell.

4.2.1 Method description

A family of impulse responses for various levels of SOC are calculated and stored in a look-up table. In other words the whole available range of SOC of the battery is being partitioned by i individual values corresponding to a specific impulse response ($h_i[k]$). The

input current is applied to the battery experimentally and the battery voltage response to that specific current is measured.

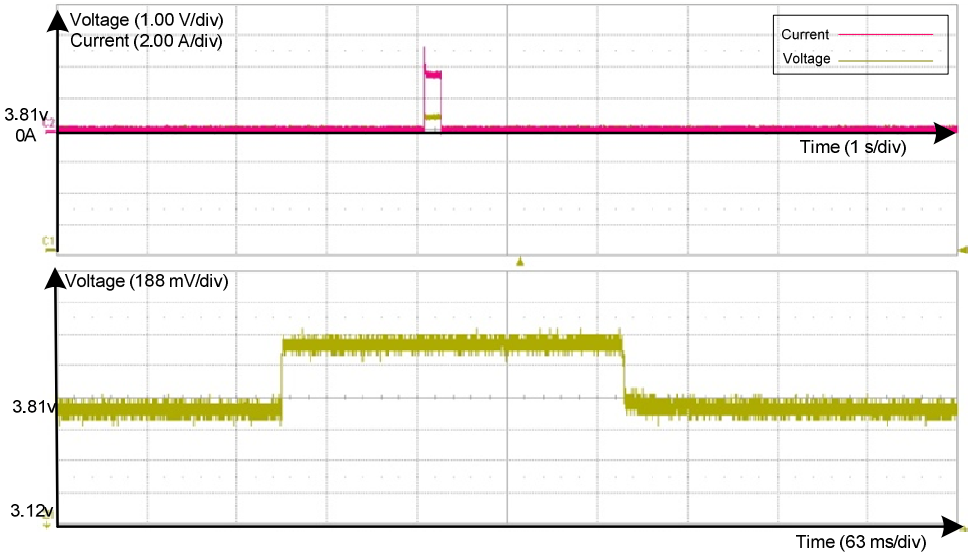

(a)

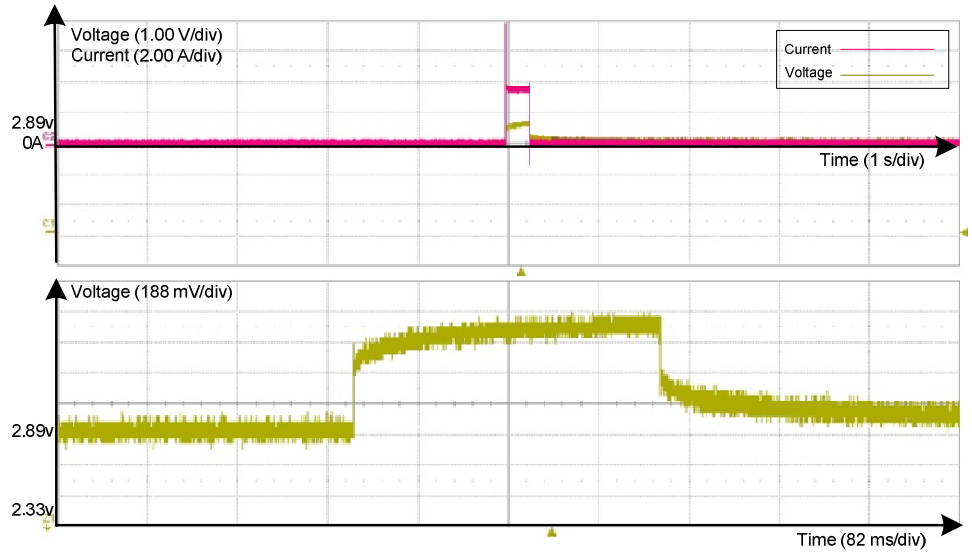

(b)

Figure 4.2 Impulse responses of the experimental cell for various SOCs. (a) battery impulse response when SOC = 75% and (b) battery impulse response when SOC = 20%.

Having the impulse response of the battery stored in a look up table, the terminal voltage for an arbitrary input current can be calculated by convolution of the input current with

all the impulse responses stored in the look-up table. So, for an arbitrary input a set of i output voltages can be achieved as follows:

$$v_i[k] = i[k] * h_i[k] \Rightarrow v_i[k] = \sum_{j=1}^{N} i[j] * h_i[k-j] \tag{4.1}$$

Comparing the measured output voltage and the calculated voltages using the impulse responses from the look-up table using the Fitness function introduced in section 3.3.2, the proper impulse response related to the battery would be determined. As the SOC corresponding to each impulse response is known, the state-of-charge of the battery can be determined. Figure 4.3 shows the block diagram of the proposed method [45].

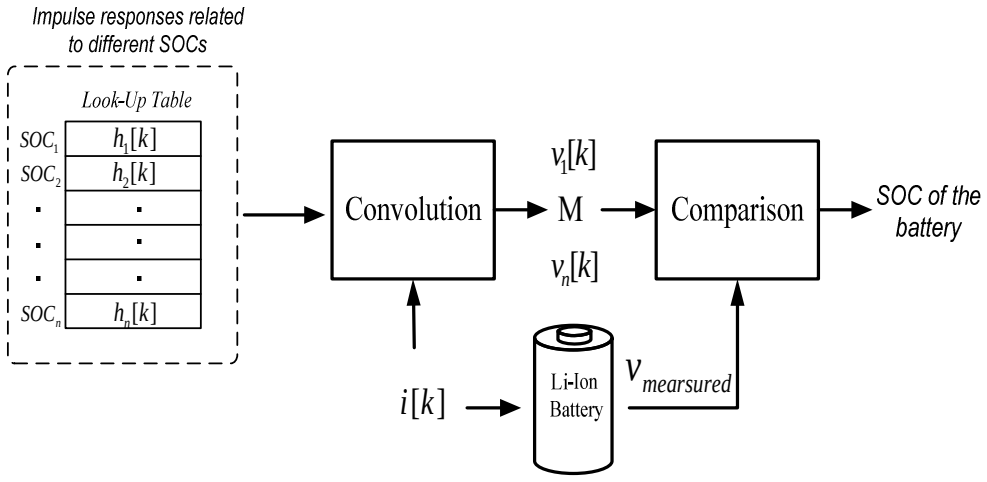

Figure 4.3 Block diagram of the state-of-charge estimation method.

4.2.2 Experimental Results

The battery type which is used for the experimental results is 26650 Li-Ion. The impulse responses of the battery corresponding to different state-of-charges are calculated using the system identification toolbox in MATLAB® v7.6. A discharging current of 2.2A for 10sec is applied to the cell while the SOC is 100%, 60%, and 20%. Figure 4.4 shows the applied current and measured output voltage of the battery for SOC of 20%.

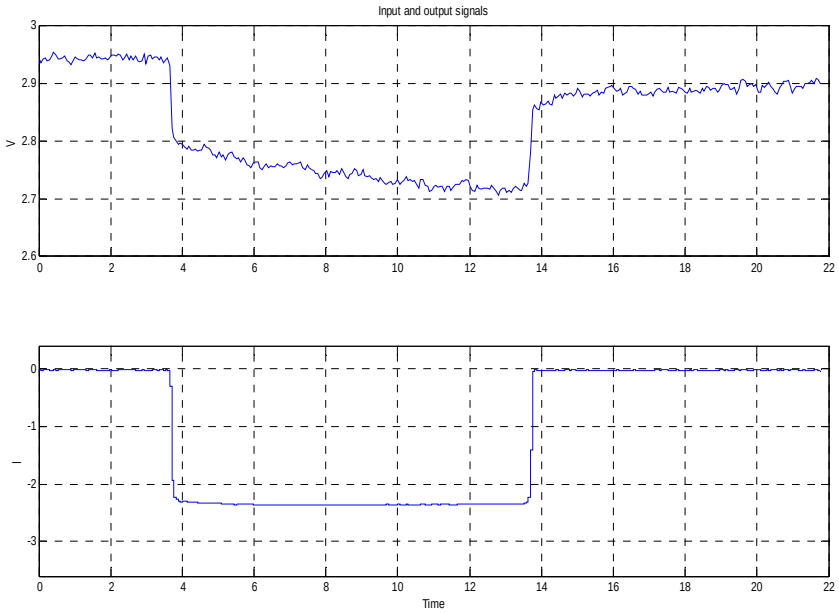

Figure 4.4 Applied current and measured voltage of the experimental cell, SOC = 20%.

Using the current and voltage waveforms in Figure 4.4, the impulse response of the battery under test is estimated for SOC of 20%. Impulse responses corresponding to other values of SOC are calculated using the same method. The estimated impulse response of the battery for SOC of 60% is shown in Figure 4.5. The coefficients of the impulse response is stored and convolved by any current input to form the output voltage of the battery with the SOC of 60%.

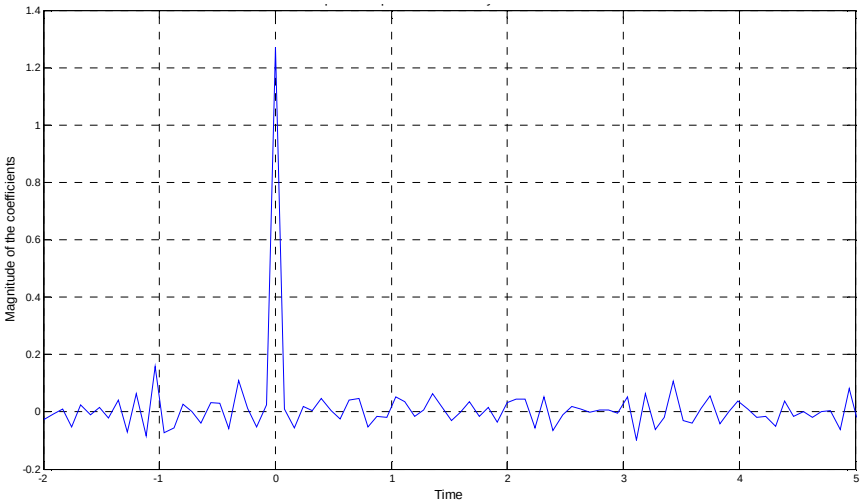

Figure 4.5 Calculated impulse response of the experimental battery, SOC = 60%.

To validate the proposed method, the calculated impulse responses corresponding to different state-of-charges need to be validated and their convolution results need to be compared to the real data measured from the battery. A pulse of 2.3A current is applied to the 26650 Li-Ion battery and the output voltage waveform is measured and stored. The same current waveform is convolved with the impulse responses of the battery for three various state-of-charges (20%, 60%, and 100%). Then, the results of the convolutions are compared to the measured voltage of the battery in order to determine the minimum error and the maximum match to the real data.

Figure 4.6 shows the comparison of measured output voltage of the experimental battery to the calculated output voltages using various impulse responses corresponding to different state-of-charges. As it is shown in this figure, data calculated by the impulse response corresponding to SOC of 100% has the best fit to the measured data (94%), whereas the other two impulse responses corresponding to SOCs of 60% and 20% have low fitting percentage (76% and 64% respectively).

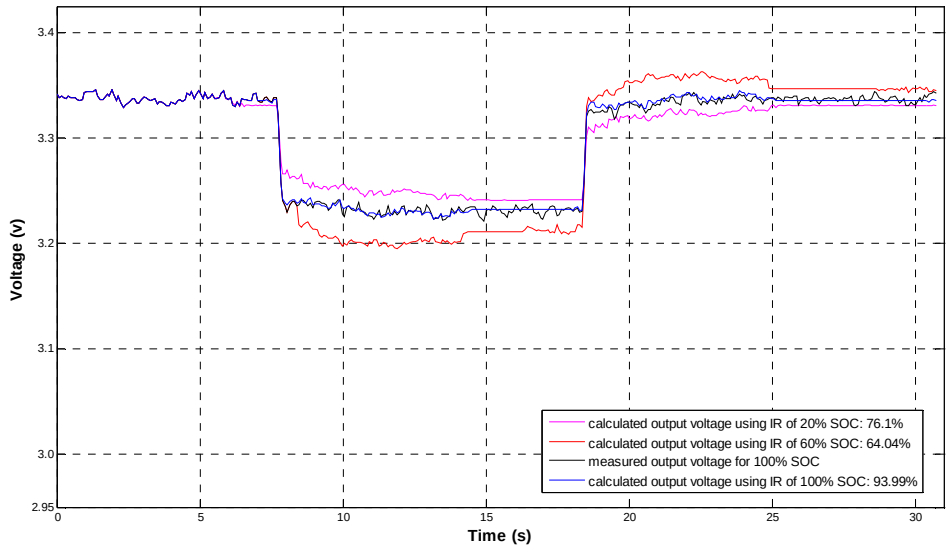

Figure 4.6 Comparison of the measured voltage of the battery for SOC = 100% with the calculated voltages for SOCs of 100%, 60%, and 20%.

Figure 4.7 compares the measured output voltage of the battery for SOC of 60% to the calculated output voltages using various impulse responses corresponding to state-of-charges of 100%, 60% and 20%. The calculated data using the impulse response of the battery for the SOC of 60% fits best to the real data (91.1%) comparing to the calculated data using other impulse responses (75% of fitting for SOC of 100% and 59% of fitting for SOC of 20%).

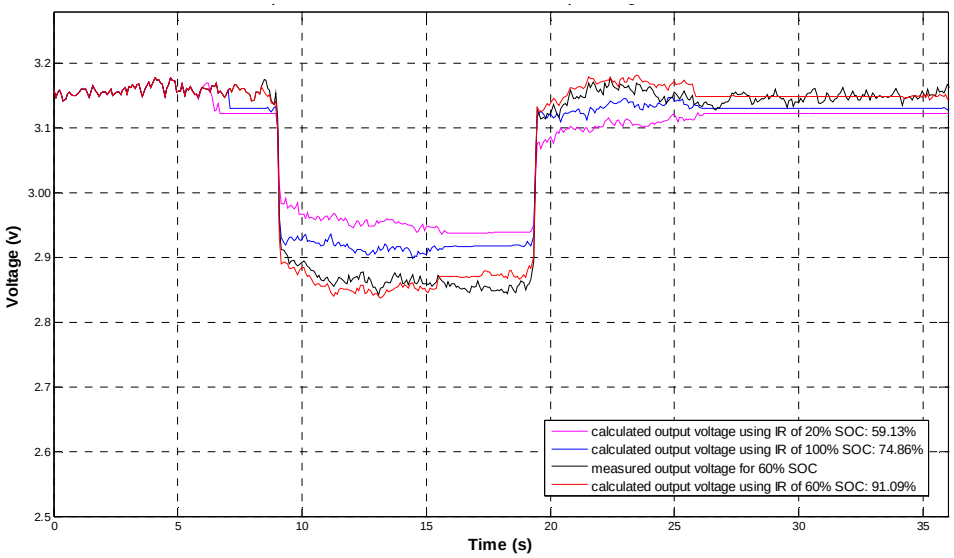

Figure 4.7 Comparison of the measured voltage of the experimental battery for SOC = 60% with the calculated voltages for SOCs of 100%, 60%, and 20%.

In Figure 4.8 the measured voltage of the battery with SOC of 20% for applying a discharge current of 2.5A for 10s is compared to the calculated output voltages using impulse responses of various SOCs of 100%, 60% and 20%. Figure 4.9 shows the same comparison as Figure 4.8, but this time the comparison is for the results of applying two discharging cycles of 5s and 15s. It is obvious that the impulse response corresponding to 20% of SOC results in higher accuracy comparing to the other two impulse responses for SOCs of 100% and 60%.

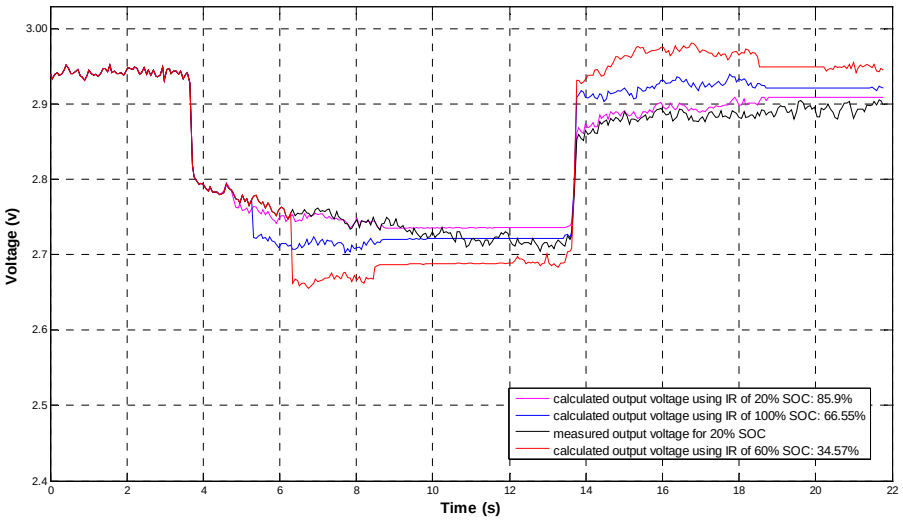

Figure 4.8 Comparison of measured output voltage of the experimental battery with SOC of 20% with the calculated voltages for SOCs of 100%, 60%, and 20%.

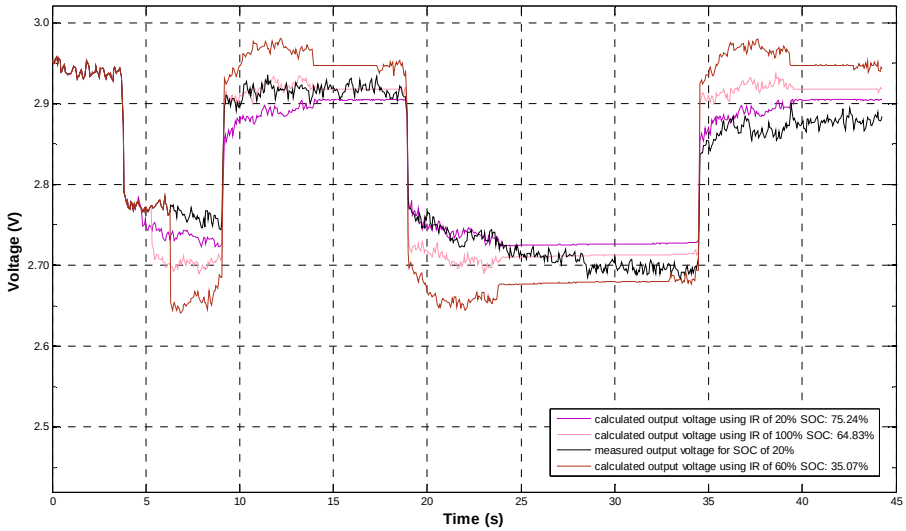

Figure 4.9 Comparison of the measured voltage of the experimental battery for SOC =20% for two discharging cycles with the calculated voltages for SOCs of 100%, 60% and 20%.

4.3 Battery Management System Development

Monitoring the status of the battery is crucial for energy storage system of Electric and Hybrid Electric Vehicles (EV/HEV). Li-Ion batteries, specifically, need an accurate monitoring and control system because of their specific characteristics. Deep discharging and overcharging of these batteries reduces their lifetime and overcharging them may cause overheating or even

explosion. The overcharge voltage is not too much higher than the fully charged voltage, which means it requires precise monitoring of voltage during charging process in order to let the battery to be charged completely while preventing overcharging. Also their temperature should be monitored continuously to recognize possible faults and accomplish the appropriate treatment if necessary.

A monitoring circuit has been designed in this project which monitors the temperatures and voltages of a battery pack consist of six 18650 Li-Ion batteries which are connected in series. The circuit measures the individual voltages and temperatures of six cells and also the voltage and current of the battery pack. Figure 4.10 shows the block diagram of the monitoring circuit.

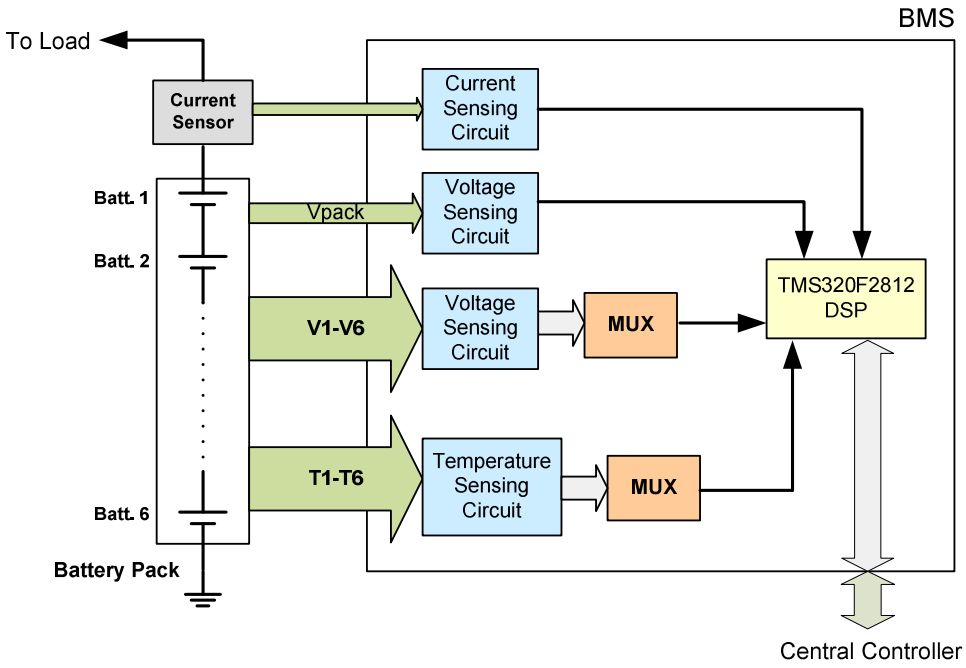

Figure 4.10 Block diagram of the monitoring circuit.

The six individual signals related to the voltages and temperatures of the batteries are sent to the Battery Management System (BMS) board. The corresponding sensing circuits measure the voltage and temperature values. Because of the limitations in analog (A/D) inputs of the DSP controller, two individual 8 to 1 multiplexers are used to select one signal per time

out of 12 values of voltage and temperature (one 8 to 1 multiplexer for voltage and another one for temperature values). A current sensor is mounted on the way of the outgoing current from the battery pack which along with the current sensing circuit on the battery monitoring board creates specific signals based on the magnitude of the current. The produced signal is sent to the DSP board and the corresponding current magnitude is calculated and transferred to the central controller.

The control routines for the system is developed using a DSP controller, TMS320F2812, to produce controlling signals and submit the sensor data to a central controller. The central controller in this case is a personal computer. Figure 4.12 illustrates the controller board, battery pack and the monitoring (BMS) board.

4.4 Test bed Development

In order to validate the potential capabilities of the proposed method for state-of-charge estimation, a 40kwh Li-Ion battery pack for EV/HEV applications is developed and examined at Renewable Energy and Vehicular Technology Lab. The following tasks are accomplished using the experimental test bed:

- A battery management system is designed and validated to monitor currents of both branches, temperatures and voltages of the individual cells and also the voltage of the battery pack
- The proposed state-of-charge estimation method is validated for the cells inside the battery pack. The required routine for this purpose is implemented and tested using TMS320F2812 DSP which is used as the main controller of the Battery Management System of the test bed.

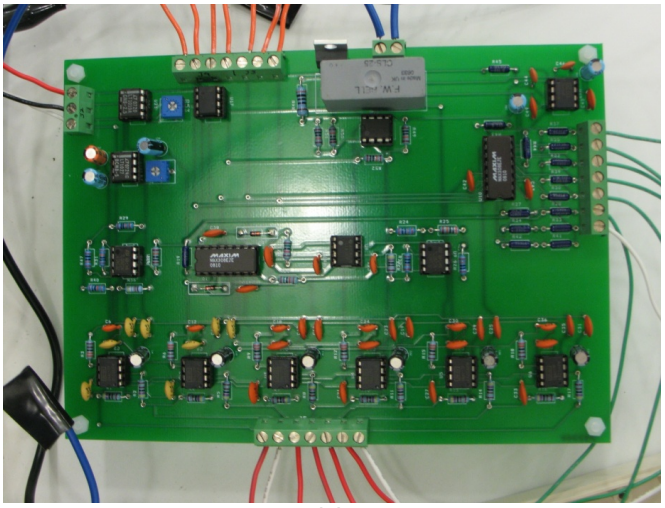

(a)

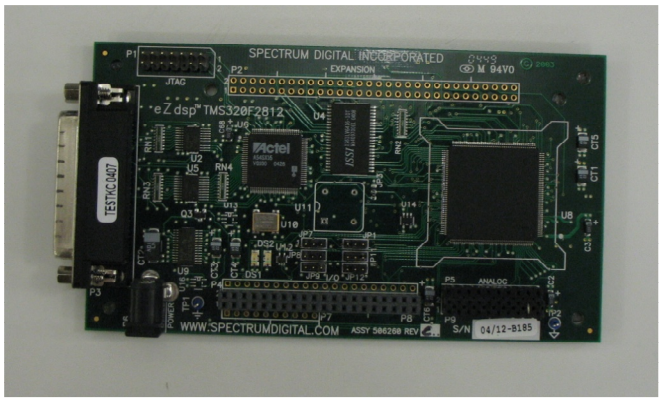

(b)

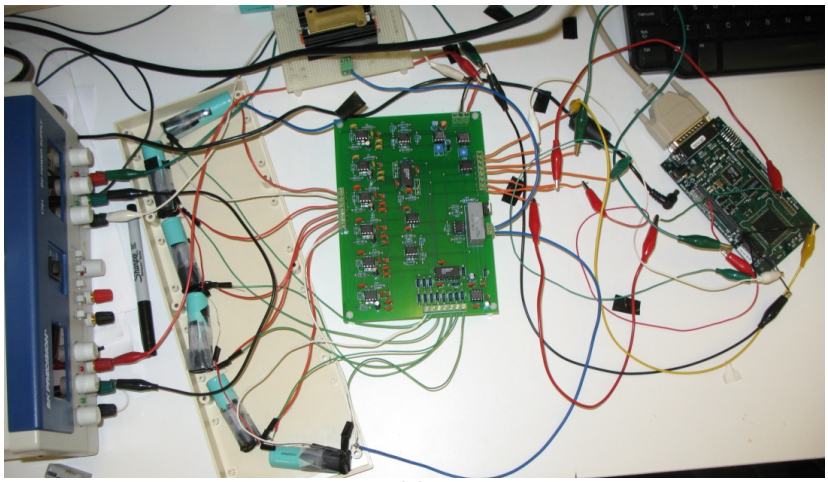

(c)

Figure 4.11 The battery monitoring system for a battery pack containing six 18650 Li-Ion cells. (a) designed Battery Management System board, (b) TMS320F2812 DSP board and (c) overall connections of the power supply, battery pack and controller.

4.4.1 The battery model

The battery type which is used for battery pack development of the test bed is SE180AHA model, Li-Ion from Sky Energy CO.. Figure 4.12 shows the datasheet and a picture of the experimental battery. In order to design a 40kwh battery pack, 80 cells of the SE180AHA Li-Ion battery is required. The cells are configured in two branches of 40 cells connected in series and the two branches are connected together in parallel. Figure 4.13 depicts the configuration of the cells for the 40kwh battery pack.

4.4.2 Developed battery management system for the test bed

A battery management system is developed to monitor the key parameters of the battery pack such as temperatures, voltages of all individual batteries, the overall voltage of the battery pack and the current of two branches which are connected in series. The values of voltages and temperatures are measured using the voltage and temperature sensing circuit. Because of the limitations in the number of A/D analog inputs of the DSP controller (as mentioned in section 4.3), several multiplexes are used to select among the voltage and temperature values before sending to the DSP. The measured values are displayed on a touch screen.

The BMS is controlled by TMS320F2812 DSP board (Figure 4.11(b)). An external memory chip (M45PE10, 1Mbit) is used in case of shortage in DSP board memory space for saving the impulse response coefficients. It is also responsible for storing the critical values such as state-of-charge of the batteries every time the system is turned off and loading the values to the DSP for the next start up. A real time clock is responsible to keep the time even when the system is off. Figure 4.14 depicts the block diagram of the developed battery management system.

MODEL:SE180AHA		
Nominal Capacity	180Ah	
Energy Density	105Wh/kg@0.1C	
Operating Voltage	Charge	3.6V
	Discharge	2.0V
Max Charge Current	≤3CA	
Max Discharge Current	Constant Current	≤4CA
	Impulse Current	≤12CA
Standard Charge /Discharge Current	0.3CA	
Operating Temperature	Charge	0℃～55℃
	Discharge	-25℃～55℃
Self-discharge Rate	≤3%(Monthly)	
Weight	5.6kg±0.1kg	

(a)

(b)

Figure 4.12 The SE180AHA Li-Ion battery specifications. (a) battery specifications and (b) the experimental battery.

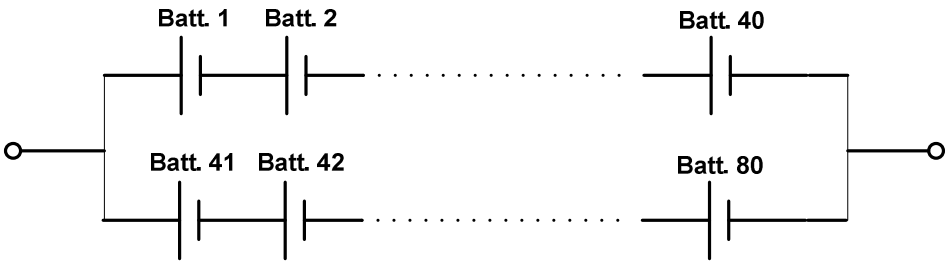

Figure 4.13 The cell configuration for 40kwh battery pack.

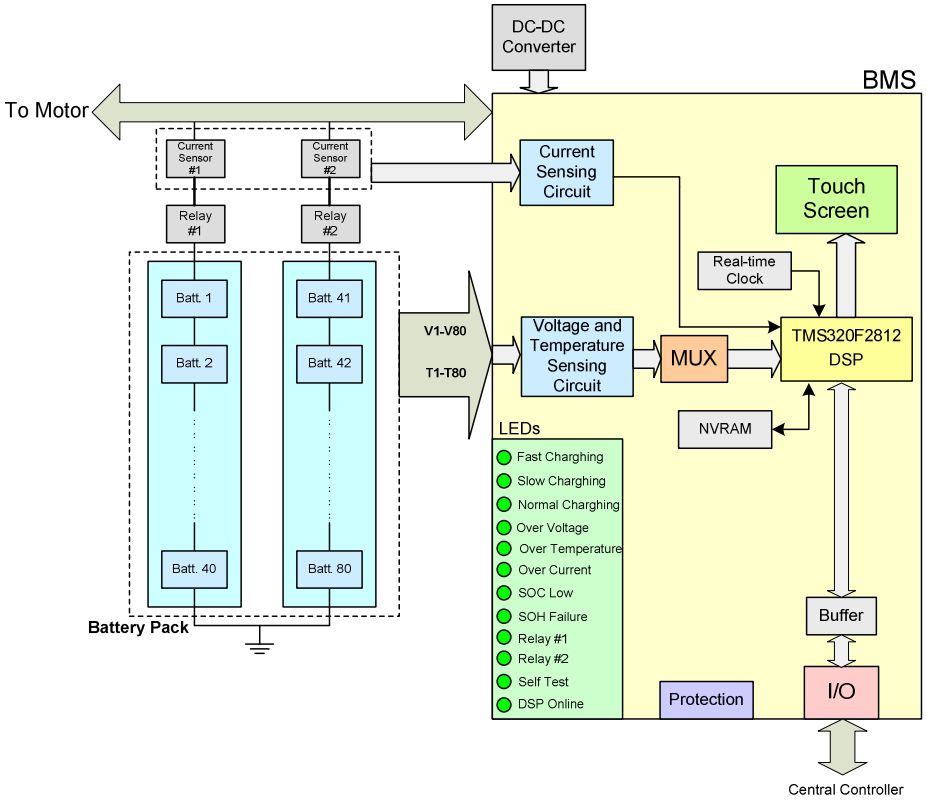

Figure 4.14 The schematic of the developed battery management system.

Figure 4.15 shows the designed PCB boards for the battery management system which contains two separate boards. The bottom board includes the voltage sensing circuits for 80 individual cells and the board on top contains various components including the temperature sensing circuits for 80 cells, current sensing circuit, real time clock, external memory chip and several LEDs indicating different situations.

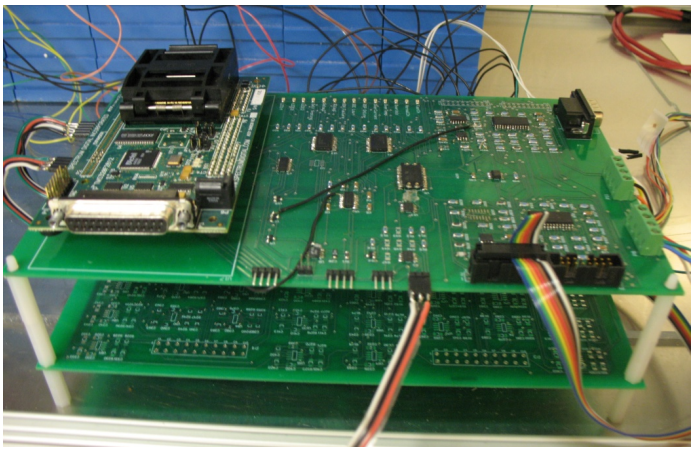

(a)

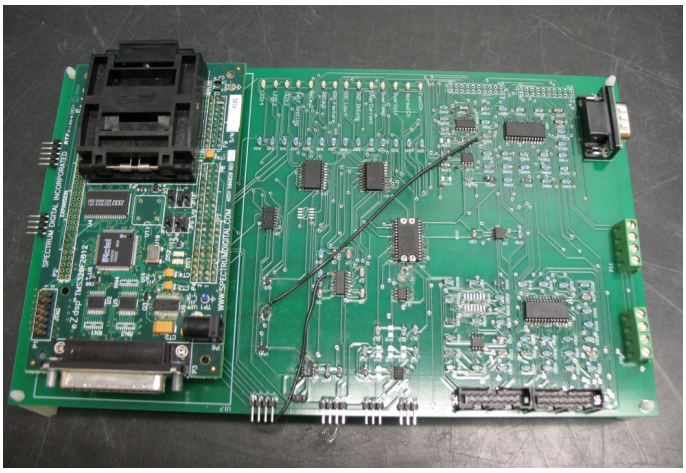

(b)

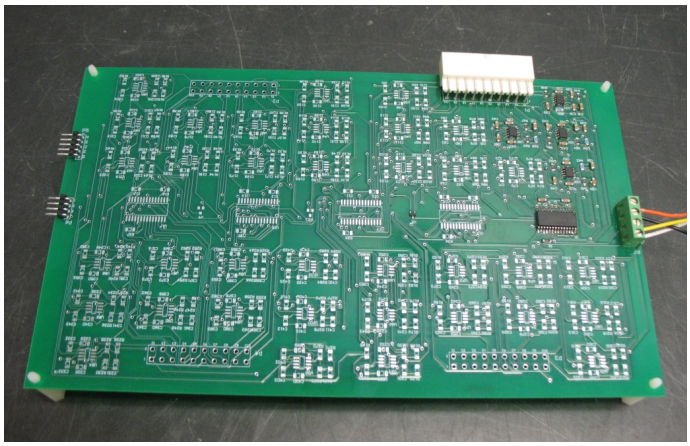

(c)

Figure 4.15 The battery management system boards. (a) the board stack, (b) the current and temperature sensing and controller board and (c) the voltage sensing board.

The top board also includes the DSP board to receive measured signals and display the values on a touch screen and to issue control signals for various components all over the boards. There is also a touch screen which is responsible to display the values of temperatures, voltages, currents and state-of-charges for all of the cells of the battery pack.

The overall view of the test bed is depicted in Figure 4.16. The battery pack, the BMS boards, touch screen and the power supply are shown in Figure 4.17(a) and the load and current sensor are shown in Figure 4.17(b). Because of the limitation in the number of available batteries in the lab, it was only possible to make a 4kwh battery pack by connecting eight cells in series.

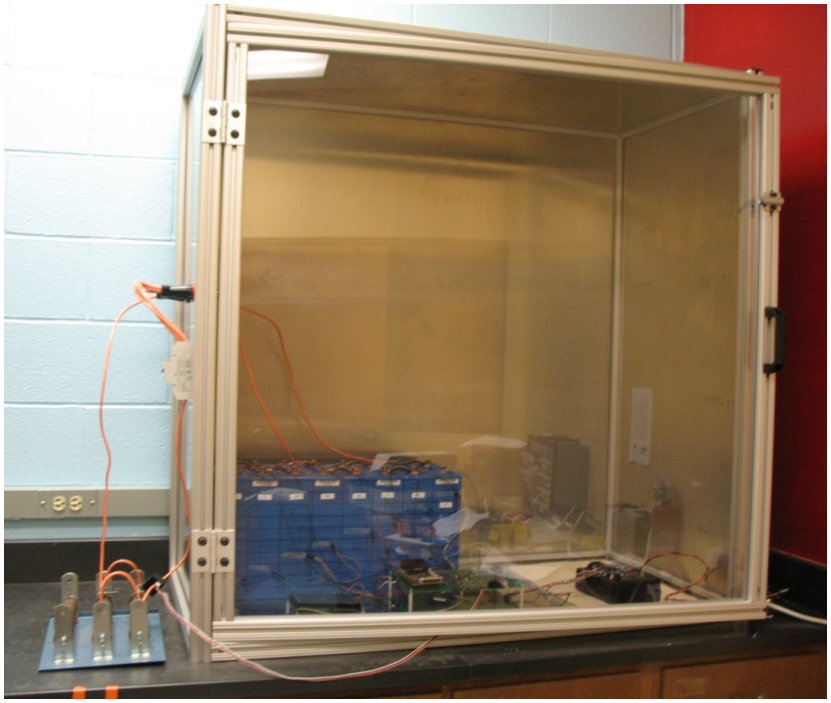

Figure 4.16 The overall view of the experimental test bed.

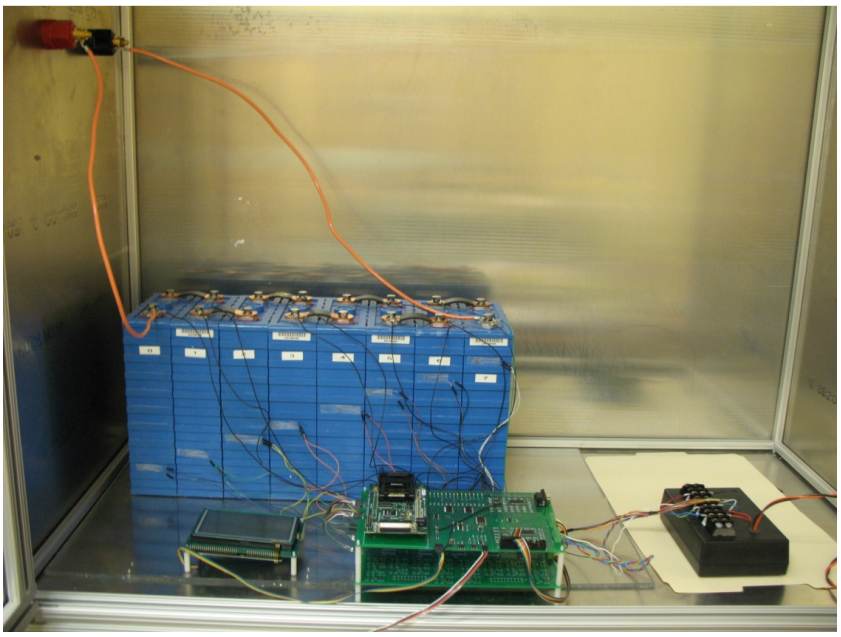

(a)

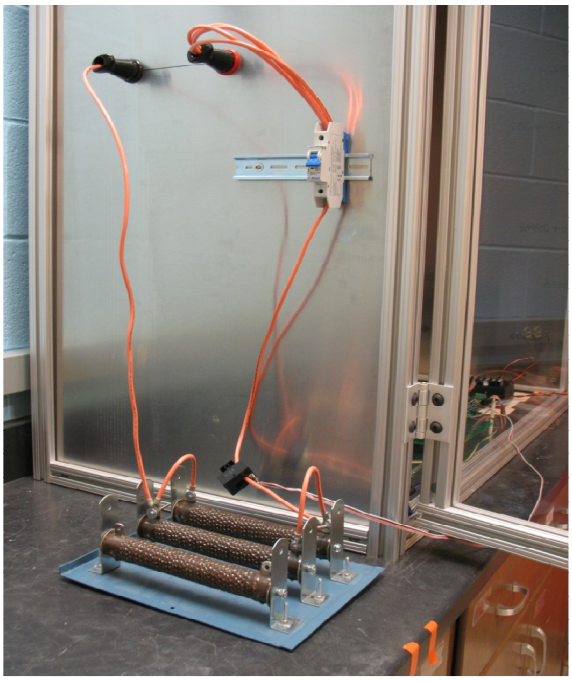

(b)

Figure 4.17 The experimental test bed. (a) battery pack, BMS boards, touch screen and power supply and (b) the load and current sensor.

4.4.3 Experimental results

To validate the state-of-charge estimation method explained in section 4.2 the experimental test bed is used. The impulse response coefficients corresponding to various state-of-charges are calculated and stored in DSP. For the specific load connected to the battery pack, the current and voltage values are measured and stored using the sensing circuits on BMS board. For the current waveform applied to the battery pack the voltage response of the batteries are calculated using the impulse response coefficients, and compared to the measured voltages using the fitness function introduced in section 3.3.2. Comparing the Fitness percentage of the calculated voltages corresponding to various state-of-charges for each individual battery inside the battery pack, the state-of-charge of that specific cell is estimated. All the control and diagnostic routines are written in DSP programming language.

Figure 4.18 shows the comparison of the measured voltage for the case of a cell from the battery pack with the SOC of 90% and the calculated voltages for the impulse responses corresponding to the state-of-charges of 90% and 50%. The applied current waveform to the battery pack is shown in Figure 4.18(a) which includes two discharging pulse with the lengths of 5s and 15s and the magnitudes of 48A. The comparison of the measured and calculated voltage is shown in Figure 4.18(b). As it is shown in the figure the fitness percentage for the waveforms corresponding to 90% and 50% of SOC are 89% and 45% relatively.

Figure 4.19 depicts the comparison of the measured and calculated voltages of the same case as Figure 4.18, but this time for applying one discharging current of 48A and with the length of 10s. Based on the Fitness values shown in the figure, the state-of-charge of the battery is estimated as 90%.

The same comparisons as Figures 4.18 and 4.19 are done in Figure 4.20 for the case of a battery with the state-of-charge of 50%. Figure 4.20(a) shows the comparison of the measured and calculated voltages for applying the input current waveform of Figure 4.18(a) and Figure 4.20(b) depicts the comparison of voltages for the input current shown in Figure 4.19(a).

Comparing the Fitness percentages of the calculated voltages creates a proper estimation for the state-of-charge of the specific cell of the battery pack.

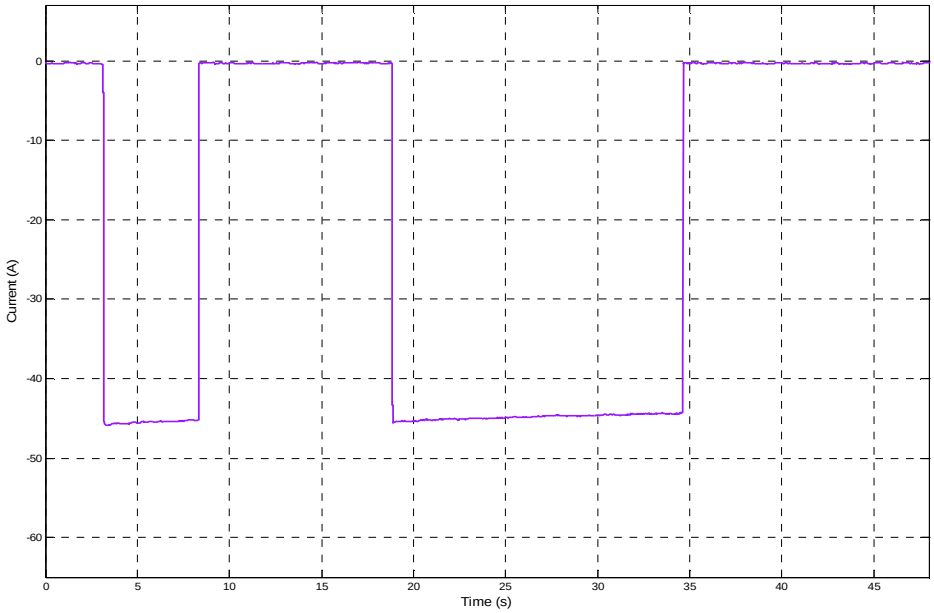

(a)

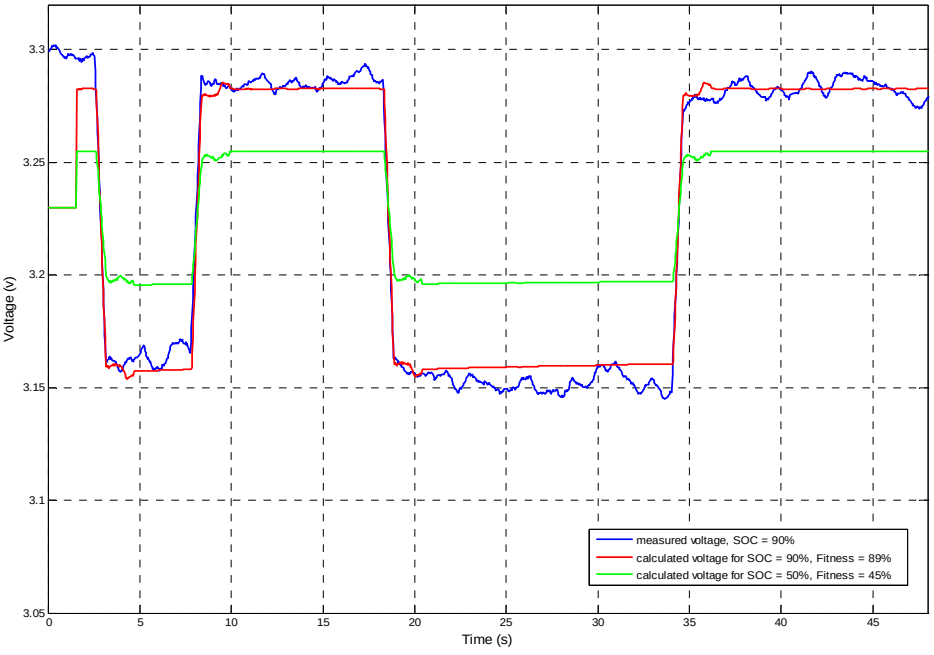

(b)

Figure 4.18 Comparison of the measured and calculated voltages for the cell with SOC of 90% for two discharging pulses. (a) applied current waveform and (b) voltage comparison.

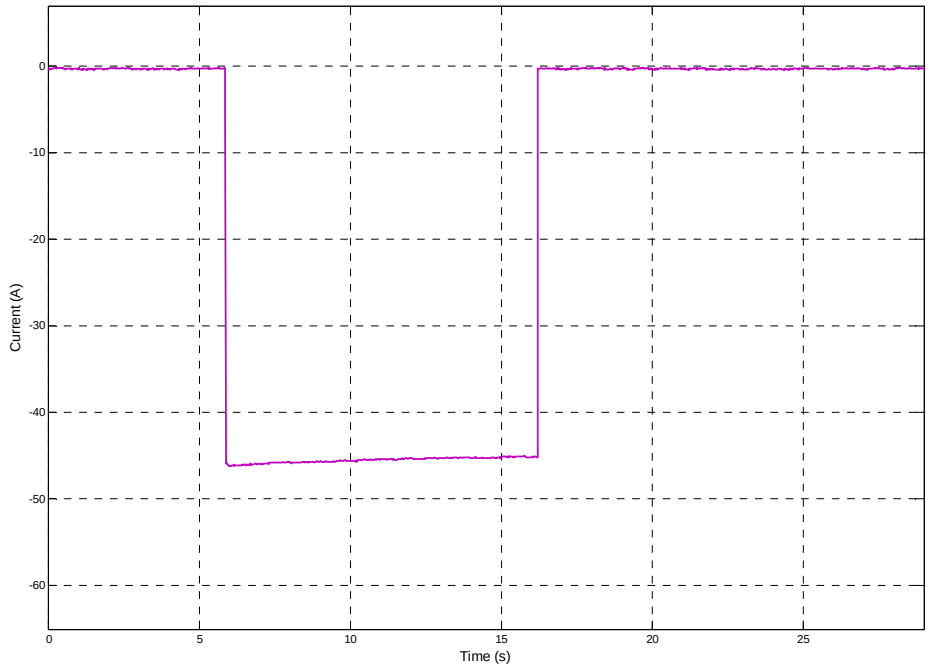

(a)

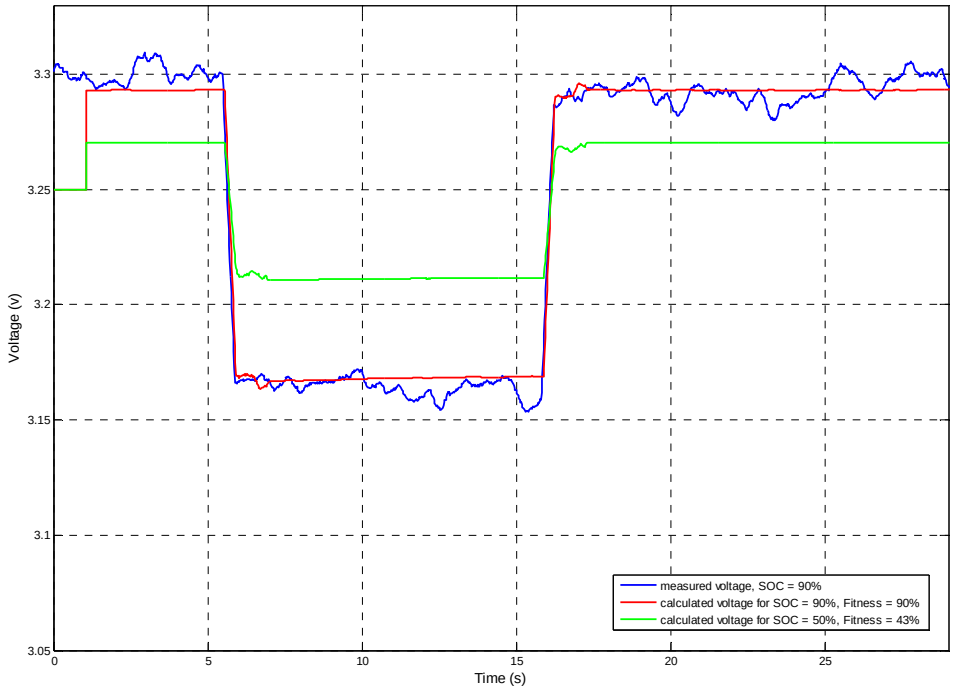

(b)

Figure 4.19 Comparison of the measured and calculated voltages for the cell with SOC of 90% for one discharging pulse. (a) applied current waveform and (b) voltage comparison.

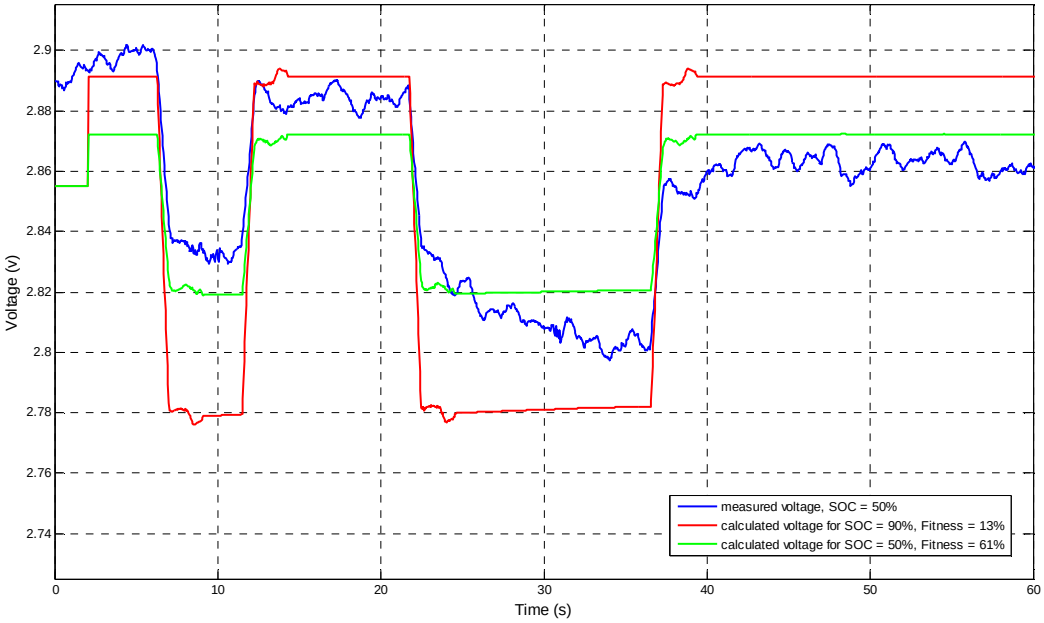

(a)

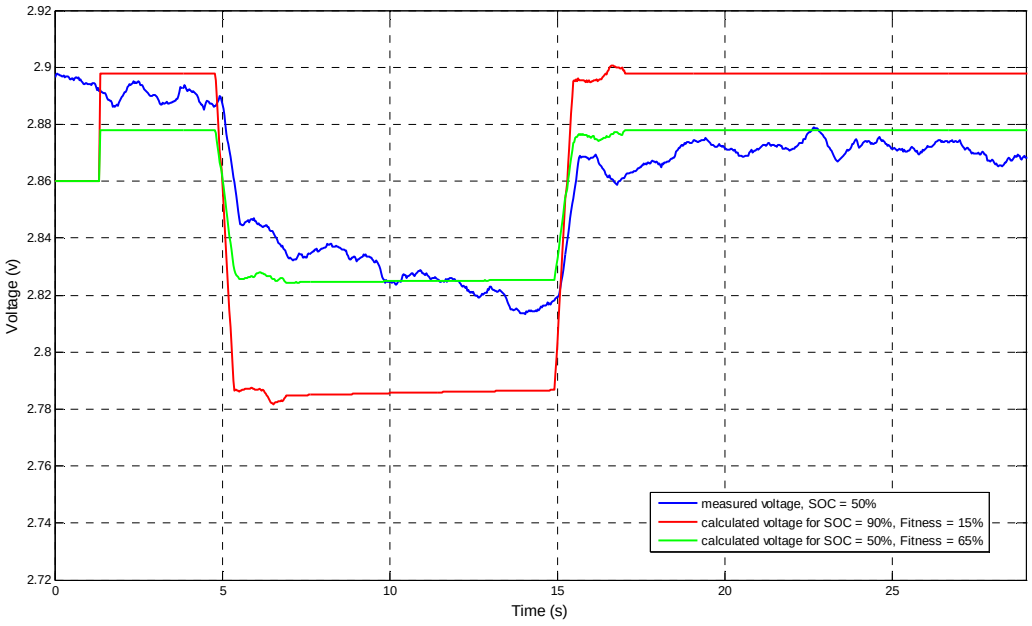

(b)

Figure 4.20 Comparison of the measured and calculated voltages for the cell with SOC of 50%. (a) voltage comparison for two discharging current pulses and (b) voltage comparison for one discharging current pulse.

CHAPTER 5

CONCLUSIONS

Monitoring the key parameters of the batteries is crucial in Electric and Hybrid Electric applications (EV/HEV). Battery management system is responsible to monitor the temperature, current and voltage of individual batteries inside the battery pack. State-of-charge and state-of-health estimations are the basic requirements for the battery management systems.

In this dissertation, a state-of-health detection method has been developed for Li-Ion batteries. This method models the battery using its impulse response and predicts the terminal voltage of the battery by convolving the input current with the impulse response of the battery. Because of the dependency of the impulse response to the health condition and the possible fault of the cell, the developed method is able to detect the type of the fault, lifetime and health condition of the individual cells inside the battery pack. This method has the ability of online detection of the health status of the battery which is in high importance for vehicular technologies and it can be modified for other types of battery chemistry.

A state-of-charge estimation method for Li-Ion batteries is also developed in this dissertation which is based on the impulse response of the battery. The relationship of the battery state-of-charge to its impulse response is applied in this method. The voltages corresponding to various state-of-charges are calculated using their relative impulse responses and compared to the terminal voltage of the battery. The developed method is capable of estimating the state-of-charge of the battery in real time and it can be modified for any other battery chemistries. The developed methods are verified by the simulation and experimental results.

For future work, it is suggested to develop a method for quantifying the life time of the battery. The mentioned method could use the detected fault along with the Fitness percentage to determine the available time to utilize the battery. The required Fitness percentage for this purpose is acquired by comparing the battery output voltage with the voltage calculated using the impulse response of the healthy battery. It is also recommended to develop a method to compress the impulse responses coefficients in order to reduce the required memory for storing the impulse responses.

REFERENCES

[1] D. Linden, T.B. Reddy, *Handbook of Batteries*, McGraw-Hill, 2002.

[2] T. Osaka, M. Datta, *Energy Storage Systems for Electronics*, Gordon and Breach Science Publishers, 2000.

[3] J. P. Aditya, M. Ferdowsi, "Comparison of Ni-MH and Li-Ion batteries in automotive applications", *IEEE Int. Conf. Vehicle Power and Propulsion*, *VPPC'08,* pp. 1-6, 2008.

[4] P. M. Gomadam, J. W. Weidner, R. A. Dougal, R. E. White, "Mathematical modeling of lithium-ion and nickel battery systems", *J. Power Sources,* 110, 267–284, 2002.

[5] V. Pop, H. J. Bergveld, J. H. G. Op het Veld, P. P. L. Regtien, D. Danilov, P. H. L. Notten, "Modeling battery behavior for accurate State-of-Charge indication", *J. Electrochem. Soc.*, Vol. 153, No. 11, pp. A2013-A2022, 2006.

[6] A. Affanni, A. Bellini, G. Franceschini, P. Guglielmi, C. Tassaoni, "Battery choice and management for new-generation electric vehicles", *IEEE Trans. Industrial Electronics*, Volume 52, No. 5, pp. 1343-1349, 2005.

[7] V. Pop, H. J. Bergveld, P. P. L. Regtien, J. H. G. Veld, D. Danilov, P. H. L. Notten, "Battery aging and its influence on the electromotive force", *J. Electrochem. Soc.*, Vol. 154, No. 8, pp. A744-A750, 2007.

[8] A. Szumanowski, Y. Chang, "Battery Management System Based on Battery Nonlinear Dynamics Modeling", *IEEE Trans. Veh. Technol.,* Volume 57, Issue 3, pp. 1425-1432, 2008.

[9] B. Tsenter, "Battery Management for Hybrid Electric Vehicle and Telecommunication Applications", *IEEE The 17th Annual Battery Conf. on Applications and Advances*, pp. 233-237, 2002.

[10] V. Pop, H.J. Bergveld, P.H.L Notten, P.P.L Regtien, “Smart and Accurate State-of-Charge Indication In Portable Applications”, *IEEE Int. Conf. on Power Electronics and Drives Systems*, *PEDS’05,* Volume 1, pp. 262-267, 2005.

[11] K. Onda, M. Nakayama, K. Fukuda, K. Wakahara and T. Araki, “Cell Impedance Measurement by Laplace Transformation of Charge or Discharge Current–Voltage”, *J. Electrochem. Soc.*, 153 (6), A1012-A1018, 2006.

[12] J. H. Kim, S. J. Lee, J. M. Lee, B. H. Cho, “A New Direct Current Internal Resistance and State of Charge Relationship for the Li-Ion Battery Pulse Power Estimation”, *IEEE 7th Int. Conf. Power Electronics*, *ICPE’07,* Volume 52, Issue 5, pp. 1173-1178, 2007.

[13] P. Shi, C. Bu, Y. Zhao, “The ANN Models for SOC/BRC Estimation of Li-ion Battery”, *IEEE Int. Conf. Information acquisition*, pp. 560-564, 2005.

[14] R. E. Garcia, Y. M. Chiang, W. C. Carter, P. Limthongkul, C. M. Bishop, “Microstructural Modeling and Design of rechargeable Lithium-Ion Batteries”, *J. Electrochem. Soc.*, 152 (1), A255-A263, 2005.

[15] H. Yang, C. M. Huang, C.L.Huang, “Identification of ARMAX Model for Short Term Load Forecasting: An Evolutionary Programming Approach”, *IEEE Trans. Power Systems*, Volume 11, No. 1, pp. 403-408, 1996.

[16] M. Ragsdale, J. Brunet, B. Fahimi, “A Novel Battery Identification Method Based on Pattern Recognition”, *IEEE Int. Conf. Vehicle Power and Propulsion*, *VPPC’08,* pp. 1-6, 2008.

[17] M. Keralu, J. Reimer, E. Cairns, “Layered nickel oxide-based cathodes for lithium cells: Analysis of performance loss mechanisms”, *J. Electrochem. Soc.*, Vol. 152, No. 8, pp. A1629-A1632, 2005.

[18] J. Christensen, J. Newman, “A mathematical model for the Lithium-ion negative electrode solid electrolyte interphase”, *J. Electrochem. Soc.*, Vol. 151, No. 11, pp. A1977-A1988, 2004.

[19] J. P. Christophersen, C. D. Ho, C. G. Motloch, D. Howell, H. L. Hess, “Effects of reference performance testing during aging using commercial Lithium-ion cells”, *J. Electrochem. Soc.*, Vol. 153, No. 7, pp. A1406-A1416, 2006.

[20] P. Ramadass, B. Haran, P. M. Gomadam, R. White, B. N. Popov, “Development of first principles capacity fade model for Li-ion cells”, *J. Electrochem. Soc.*, Vol. 151, No. 2, pp. A196-A203, 2004.

[21] C. S. C. Bose, F. C. Laman, “Battery state of health estimation through Coup De Fouet”, *IEEE The 2nd Annual of Telecommunications Energy Conference, INTELLEC’00*, pp. 597-601, 2000.

[22] F. Olivier, M. Didier, “Testing battery state of health with portable metering devices?”, *IEEE The 9th Annual of Telecommunications Energy Conference, INTELLEC’07,* pp. 203-209, 2007.

[23] S. Brown, N. Mellgren, M. Vynnycky and G. Lindbergha, **“**Impedance as a tool for investigating aging in Lithium-ion porous electrodes, II. Positive electrode examination”, *J. Electrochem. Soc.*, Vol. 155, No. 4, pp. A320-A338, 2008.

[24] M. Keralu, R. Kostecki, “Interfacial impedance study of Li-Ion composite cathodes during aging at elevated temperatures”, *J. Electrochem. Soc.*, Vol. 153, No. 9, pp. A1644-A1648, 2006.

[25] F. Huet, “A review of impedance measurements for determination of the state-of-charge or state of health of secondary batteries”, *J. Power Sources*, Vol. 70, pp. 59-69, 1998.

[26] C. S. C. Bose, D. Wilkins, S. McCluer, M. J. Model, “Lessons learned in using ohmic techniques for battery monitoring”, *IEEE The 6th Battery Conference on Applications and Advantages,* pp. 99-104, 2001.

[27] H. Miyamoto, M. Morimoto, K. Morita, “On-line SOC estimation of battery for wireless tram car”, *IEEE Int. Conf. Power Electronics and Drive Systems, PEDS’07,* pp. 1624-1627, 2007.

[28] H. J Bergveld, W. S. Kruijit, P. H. L. Notten, *Battery Management Systems, Design by Modeling,* Philips Research Book Series, Vol. 1, Kluwer Academic Publishers, Boston, 2002.

[29] C. Speltino, D. Di Domenico, G. Fiengo, A. Stefanopoulou, "Comparison of reduced order Lithium-Ion battery models for control applications", *IEEE The 48th Annual of Design and Control*, pp. 3276-3281, 2009.

[30] V. Srinivasan, G. Q. Wang, C. Y. Wang, "Mathematical modeling of current-interrupt and pulse operation of valve-regulated Lead-Acid batteries", *J. Electrochem. Soc.*, Vol. 150, No. 3, pp. A316-A325, 2003.

[31] S.X. Chen, K.J. Tseng, S.S. Choi, "Modeling of lithium-ion battery for energy storage system simulation", *IEEE Power and Energy Engineering Conferences, APPEEC*, pp. 1-4, 2009.

[32] N. K. Modera, A. Kusko, "An enhanced dynamic battery model of Lead-Acid batteries using manufacturers' data", *IEEE The 28th Annual of Telecommunications Energy Conference, INTELEC'06*, pp. 1-6, 2006.

[33] J.F.A. Leao, L.V. Hartmann, M.B.R. Correa, A.M.N. Lima, "Lead-Acid battery modeling and state of charge monitoring", *IEEE The 25th Annual of Applied Power Electronics Conference and Exposition, APEC'10*, pp. 239-243, 2010.

[34] D. Cadar, D. Petreus, I. Ciocan, P. Dobra, "An improvement on empirical modeling of the batteries", *IEEE The 32nd International Spring Seminar on Electronics Technology, ISSE*, pp. 1-6, 2009.

[35] S. Barsali, M. Ceraolo, "Dynamical models of Lead-Acid batteries: implementation issues", *IEEE Trans. Energy Conversion*, Volume 17, No. 1, pp. 16-23, 2002.

[36] M. Ceraolo, "New Dynamical models of Lead-Acid batteries", *IEEE Trans. Power Systems*, Volume 15, No. 4, pp. 1184-1190, 2000.

[37] L. Gao, Sh. Liu, R. A. Dougal, “Dynamic Lithium-Ion battery model for system simulation”, *IEEE Trans. Components and Packaging Technologies*, Volume 25, No. 3, pp. 495-505, 2002.

[38] H. Dai, Z. Sun, X. Wei, “Online SOC estimation of high-power Lithium-ion batteries used on HEVs”, *IEEE Int. Conf. Vehicular Electronics and Safety, ICVES’06,* pp. 342-347, 2006.

[39] P. K. Artemiadis, K.J. Kyriakopoulos, “EMG-based teleoperation of a robot arm in planar catching movements using ARMAX model and trajectory monitoring techniques *IEEE Int. Conf. Robotics and Automation, ICRA*, pp. 3244-3249, 2006.

[40] N. K. Sinha, *Linear Systems*, John Wiley & Sons, 1991.

[41] N. Takami, H. Inagaki, T. Kishi, Y. Harada, Y. Fujita, K. Hoshina, “Electrochemical kinetics and safety of 2-volt class Li-ion battery system using lithium titanium oxide anode”, *J. Electrochem. Soc.*, Vol. 156, No. 2, pp. A128-A132, 2009.

[42] M. Ichimura, “The safety characteristics of Lithium-ion batteries for mobile phones and the nail penetration test”, *IEEE The 9th Annual of Telecommunications Energy Conference, INTELLEC’07*, pp. 687-692, 2007.

[43] J. Loud, S. Nilsson, Y. Du, “On the testing methods of simulating a cell internal short circuit for lithium ion batteries”, *IEEE The 17th Annual of Battery Conference on Applications and Advances*, pp. 205-208, 2002.

[44] A. Banaei, B. Fahimi, “Real time condition monitoring in Li-Ion batteries via battery impulse response”, Accepted and to be presented at *IEEE Int. Conf. Vehicle Power and Propulsion*, *VPPC’10,* 2010.

[45] A. Banaei, A. Khoobroo, B. Fahimi, “Online detection of terminal voltage in Li-ion batteries via battery impulse response”, *IEEE Int. Conf. Vehicle Power and Propulsion*, *VPPC’09,* pp. 194-198, 2009.

BIOGRAPHICAL INFORMATION

Anahita Banaei was born on February 2, 1981 in Boroujerd, Iran. She received her Bachelor of Science from University of Tehran, Tehran, Iran, in 2002 and Master of Science in Computer Architecture from the Isfahan University of technology, Isfahan, Iran, in 2006. She started her PhD in Fall 2007 at the University of Texas at Arlington. During her PhD, she was employed at Renewable Energy and Vehicular technology Laboratory as a Research Associate where she was involved in the design and implementation of Battery Management Systems. At the University of Texas at Arlington, she was also involved in various projects including the State-of-Charge and State-of-Health estimation of chemical batteries. Her research interests include power electronics, battery management systems, renewable energy and vehicular systems.